UNIVERSIDADE FEDERAL DE SANTA CATARINA
CENTRO TECNOLÓGICO
DEPARTAMENTO DE ENGENHARIA MECÂNICA
CURSO DE ENGENHARIA DE MATERIAIS

MILENY MASIEIRO

INVESTIGATING THE TRIBOLOGICAL BEHAVIOR OF PATTERNED SURFACES FUNCTIONALIZED WITH SOLID LUBRICANT NANOPARTICLES

FLORIANÓPOLIS
2023

MILENY MASIEIRO

INVESTIGATING THE TRIBOLOGICAL BEHAVIOR OF PATTERNED SURFACES FUNCTIONALIZED WITH SOLID LUBRICANT NANOPARTICLES

Bachelor Thesis in Materials Engineering at the Technological Center in Federal University of Santa Catarina as a requirement for the degree of Bachelor of Materials Engineering.

Advisor: Diego Berti Salvaro, Ph.D.
Co-advisor: Prof. Rodrigo Perito Cardoso, Ph.D.

FLORIANÓPOLIS
2023

Masieiro, Mileny
Investigating the tribological behavior of patterned surfaces functionalized with solid lubricant nanoparticles / Mileny Masieiro ; orientador, Diego Salvaro, coorientador, Rodrigo Cardoso, 2023.
77 p.

Trabalho de Conclusão de Curso (graduação) - Universidade Federal de Santa Catarina, Centro Tecnológico, Graduação em Engenharia de Materiais, Florianópolis, 2023.

Inclui referências.

1. Engenharia de Materiais. 2. texturização de superfície. 3. lubrificação sólida. 4. tribologia. I. Salvaro, Diego . II. Cardoso, Rodrigo . III. Universidade Federal de Santa Catarina. Graduação em Engenharia de Materiais. IV. Título.

MILENY MASIEIRO

INVESTIGATING THE INFLUENCE OF TEXTURIZATION ON THE TRIBOLOGICAL BEHAVIOR OF PATTERNED SURFACES WITH LUBRICANT NANOPARTICLES

Este Trabalho de Conclusão de Curso foi julgado adequado para obtenção do título de Engenheira de Materiais e aprovado em sua forma final pelo Curso de Graduação em Engenharia de Materiais na Universidade Federal de Santa Catarina.

Florianópolis, 01 de Dezembro de 2023.

Documento assinado digitalmente
Cristiano Binder
Data: 08/12/2023 10:48:41-0300
CPF: ***.079.129-**
Verifique as assinaturas em https://v.ufsc.br

Prof. Cristiano Binder, Dr., Eng.
Coordenador do Curso

Banca Examinadora:

Documento assinado digitalmente
Diego Berti Salvaro
Data: 07/12/2023 15:19:55-0300
CPF: ***.540.139-**
Verifique as assinaturas em https://v.ufsc.br

Diego Berti Salvaro, Dr., Eng.
Orientador
Universidade Federal de Santa Catarina

Documento assinado digitalmente
Rodrigo Perito Cardoso
Data: 07/12/2023 14:21:07-0300
CPF: ***.946.659-**
Verifique as assinaturas em https://v.ufsc.br

Prof. Rodrigo Perito Cardoso, Dr., Eng.
Coorientador
Universidade Federal de Santa Catarina

Documento assinado digitalmente
FELIPE GUSTAVO EBERSBACH
Data: 08/12/2023 15:15:06-0300
CPF: ***.118.249-**
Verifique as assinaturas em https://v.ufsc.br

Felipe Gustavo Ebersbach, Dr., Eng.
Universidade Federal de Santa Catarina

Documento assinado digitalmente
RENAN OSS GIACOMELLI
Data: 07/12/2023 14:00:22-0300
CPF: ***.180.289-**
Verifique as assinaturas em https://v.ufsc.br

Renan Oss Giacomelli, Dr., Eng.
Instituto SENAI de Inovação de Santa Catarina

Florianópolis, 2023.

ACKNOLEDMENTS

Firstly, I would like to express my gratitude to UFSC (Federal University of Santa Catarina) for providing free, high-quality public education, which has significantly shaped my experiences, knowledge, opportunities, and professional growth throughout the past years.

I extend my appreciation to my advisor, Diego Salvaro, for his invaluable guidance, unwavering support, patience, availability, and expertise. His mentorship has not only enriched this project but has also stimulated my development as a researcher, leaving a lasting impact on my academic pursuits.

I would also like to acknowledge and extend my gratitude to the collaborators of this study, Prof. Rodrigo Perito, Prof. Thierry Czerwiec, and Gregory Marcos. Firstly, for allowing and entrusting me with the opportunity to engage in research at the renowned IJL (Institute of Jean Lamour). This experience not only provided me with professional development but also ignited my interest in the subject of this study. Their contributions to this research project, including their dedication of time, valuable insights, thought-provoking discussions, and essential guidance, have been pivotal to its success.

To my family and friends for their unwavering support and encouragement.

Lastly, I extend my sincere gratitude to all those individuals whose contributions may not be explicitly mentioned here but have played a role in supporting me along this journey.

RESUMO

As perdas de energia por atrito, que representam um consumo considerável, e o desgaste dos componentes, uma das principais causas de falhas em máquinas e equipamentos, vem se tornando cada vez mais relevantes desde a Revolução Industrial, principalmente após os alertas de aceleração das mudanças do clima na Terra. Visando tornar esses processos mais eficientes, econômicos e sustentáveis, diferentes abordagens têm sido desenvolvidas e implementadas. Entre essas soluções, estão os processos de modificação de superfície e aplicação de nanotecnologia. No presente estudo foi investigado a combinação das tecnologias de texturização de superfície e de deposição de nanolubrificantes sólidos, demonstrando sua eficácia em promover maior vida útil a componentes e reduzir perdas por atrito e desgaste. Para isso foram produzidas quatro texturas utilizando a técnica de gravura a plasma a seco induzido por bombardeio de íons. Além disso, uma amostra de referência com superfície polida foi utilizada. Posteriormente, o nanolubrificante sólido, conhecido como grafite 2D turbostrático, foi depositado nas amostras por meio da técnica de drop-casting. Essa técnica de deposição garantiu uma cobertura consistente e distribuição uniforme em todas as condições de superfície. Para avaliar o comportamento tribológico das diferentes condições de superfície, foram conduzidos testes tribológicos de durabilidade. Além disso, as amostras passaram por análises detalhadas para caracterizar a topografia das diferentes texturas, mensurar a quantidade de nanolubrificante e investigar os mecanismos de desgaste. As técnicas de análise utilizadas foram interferometria óptica, microscopia óptica (MO), microscopia eletrônica de varredura (MEV), espectroscopia de energia dispersiva de raios-X (EDX), e espectroscopia Raman. Os resultados deste estudo demonstram o potencial sinérgico da texturização na lubrificação sólida para reduzir de maneira eficaz o desgaste e o atrito, desde que os parâmetros das texturas sejam cuidadosamente selecionados. Vale ressaltar que no presente estudo, as superfícies com texturas (exceto a textura H2-D100-A4) apresentaram durabilidade significativamente elevada, superando a durabilidade da superfície polida (295 N.m) em pelo menos três vezes (947 N.m), além de exibirem uma notável repetibilidade devido ao controle preciso que superfícies texturizadas proporcionam. Além disso, foi constatado que os *dimples* atuam como reservatórios de lubrificante sólido, fornecendo gradualmente esse lubrificante à medida que a superfície sofre desgaste, contribuindo para um melhor desempenho tribológico. Os mecanismos de desgaste observados sugerem que, à medida que os padrões da textura se desgastam, eles transacionam de uma condição suave para um mecanismo severo, assemelhando-se ao observado na superfície somente polida (sem texturização) com as partículas de lubrificante sólido se acumulando mais nas bordas da marca de desgaste.

Palavras-chave: texturização; lubrificação sólida; tribologia; plasma; nanopartículas.

ABSTRACT

Frictional energy losses, which represent a significant consumption of energy resources, and component's wear, one of the leading causes of failures in machinery and equipment, have been major challenges since the Industrial Revolution, mainly after the warnings of accelerating climate changes on Earth. In an effort to make processes more efficient, cost-effective, and environmentally sustainable, various approaches have been developed and implemented. Among these solutions are surface modification processes and the application of nanotechnology. In the present study, the combination of surface patterning and the deposition of solid nanolubricants was investigated, demonstrating their effectiveness in extending the lifespan of components and reducing friction and wear losses. To accomplish this, four surface patterns were produced using dry plasma induced by ion bombardment technique. Additionally, a reference sample with a mirror-polished finish was utilized. Subsequently, the solid nanolubricant, turbostratic 2D graphite, was deposited on the samples through the drop-casting technique. This deposition method ensured consistent coverage and uniform distribution across all surface conditions. To evaluate the tribological behavior of the different surface conditions, scuffing resistance testing was conducted. Furthermore, the samples underwent analyses to characterize the topography of the different patterns, measure the nanolubricant quantity, and investigate the underlying wear mechanisms. These analyses included interferometry, as well as optical microscopy (OM), scanning electron microscopy (SEM), and energy-dispersive X-ray spectroscopy (EDX), and Raman spectroscopy. The findings of this study demonstrate the synergistic potential of these two techniques when combined to effectively reduce wear and friction, under the condition that the texture parameters are carefully selected. It is worth noting that in this study, the patterned surfaces (except for pattern H2-D100-A4) exhibited exceptional durability, surpassing the durability of the common polished surface (295 N.m) by at least by three times (947 N.m), in addition to exhibiting remarkable repeatability owing to the precise surface control offered by the patterned surfaces. Furthermore, it was observed that the *dimples* act as solid lubricant reservoirs, gradually supplying this lubricant as the surface wears down, contributing to improved tribological performance. The wear mechanisms observed suggest that as the patterns wear down, they transition from a mild to a severe condition resembling the wear mechanisms observed in solely polished surface (no pattern) with the solid lubricant particles accumulating more at the edges of the tracks.

Keywords: surface texturing; solid lubrication; tribology; plasma; nanoparticles.

LIST OF FIGURES

LIST OF TABLES

ACRONYMS

A	Area Density
ABNT	Brazilian Association of Technical Standards
CDC	Carbon Derived from Carbide
COF	Friction Coefficient
D	Diameter
DC	Direct Current
EDX	Energy Dispersive X-ray Spectroscopy
Fz	Load Line
H	Height
ICP	Inductively Coupled Plasma
IJL	Institute Jean Lamour
IMN	Institute des Matériaux de Nantes Jean Rouxel
MDECR	Multi-Dipolar Electron Cyclotron Resonance
MPS	Mirror Polished Surface
OM	Optical Microscope
PECVD	Plasma-Enhanced Chemical Vapor Deposition
R	Resistance Line
RF	Radiofrequency
RIE	Reactive Ion Etching or inductively coupled plasma (ICP) reactor
SE	Secondary Electron
SEM	Scanning Electron Microscope
BSE	Backscattered Electron
UFSC	Federal University of Santa Catarina

TABLE OF CONTENTS

1 INTRODUCTION

Friction and wear play a significant role in the energy consumption and performance of mechanical components. Approximately 23% of the world's primary energy resources are consumed by friction, and approximately 80% of mechanical components fail due to wear (HOLMBERG; ERDEMIR, 2017; JOST, 2005). Consequently, there is a growing demand for minimizing friction and wear loss to achieve a lower energy dissipation, higher system efficiency, and mitigate environmental damage, and improve component's durability. Various approaches have been explored to reduce friction and wear, including modifying the component's design, employing surface coatings, utilizing lubricants, optimizing surface roughness, and performing surface texturing (SEDLAČEK; GREGORČIČ; PODGORNIK, 2017). On the present study were investigated the approaches: surface texturing combined with solid lubrication.

Surface patterning technology (also known as surface texturing technology) involves modifying the surface (without changing the material itself) to create structured arrays with specific parameters such as shape, arrangement, and size that depend on the application requirements (FARIA et al., 2020). Surface patterning has been widely explored and applied in mechanical components such as seals, bearings, piston ring components, tools and supports. In mechanical components surface patterning enhances tribological performance by modifying wear mechanisms and serving as debris traps, microbearings, and lubrication reservoirs (COBLAS et al., 2015). However, it can be employed beyond mechanical components, for example in optical applications to trap light, in biological applications for implants, and in applications that require hydrophobic surfaces like electronic components or in components for avoiding corrosion (BASHER et al., 2019; FARIA et al., 2020; CHEN et al., 2019; FAN et al., 2019; JAIN; BAJPAI, 2019).

In addition to surface texturing, solid lubricants such as molybdenum disulfide, graphene and graphite have also been studied extensively for their tribological performance. These solid lubricants with lamellar structure adhere to the surface of mechanical components or form an effective chemical reaction, creating a low-friction layer that reduces wear and improves durability. Solid lubricants are often selected over liquid lubricants as they exhibit excellent performance under extreme operating conditions, such as high or low temperatures, vacuum environments, and radiation exposure (ERDEMIR, 2001).

Having said that, there is a great potential of using a combination of techniques such as surface patterning and solid lubrication to further enhance the tribological performance of mechanical components. Surface patterning technology has been extensively studied with liquid lubricants or suspensions containing solid lubricants, but few academic studies have explored surface patterning exclusively functionalized with solid lubricants particles. Therefore, this study investigates the tribological performance of patterned surfaces functionalized with nanoparticles of 2D turbostratic graphite. The aim is to investigate the effect of distinct surface patterns on solid lubrication with a thorough understanding of the underlying mechanisms.

To achieve this objective, the patterned surfaces were produced through physical etching in collaboration with the research team, Plasmas - Procédés – Surfaces, at Institut Jean Lamour (IJL). Subsequently, nano lubricant was applied to the textured surfaces through drop-casting technique following the guidelines from a previous study (GIACOMELLI, 2020). Then, sliding friction testing was performed to evaluate the tribological behavior of the surfaces. Additionally, a range of characterization techniques, including optical interferometry, optical microscopy, scanning electron microscope (SEM), energy dispersive X-ray spectroscopy (EDX), and Raman spectroscopy were utilized to characterize the topography from the patterns, quantify the solid nanolubricant amount and distribution; further analyze the tribological behavior and identify the wear mechanisms of the distinct patterned surfaces.

The obtained results indicate that when patterned surfaces are combined with nanolubricant particles, a synergistic effect may be observed dependent on the correct selection of the pattern parameters. This combined approach has the potential to produce a more durable and reliable component compared to a conventionally polished component by modifying the wear mechanisms and the interactions within the tribosystem.

1.1 GENERAL OBJECTIVE

Investigate the effect of 2D turbostratic graphite nanolubricant particles on the tribological behavior of patterned surfaces with varying pattern parameters.

1.2 SPECIFIC OBJECTIVES

- Produce patterned samples and apply nanolubricant (2D turbostratic graphite) uniformly on the samples' surfaces.
- Characterize the nanolubricant area coverage and homogeneity of nanolubricant on the samples' surfaces.
- Determine the tribological behavior of the patterned surfaces with 2D turbostratic graphite.
- Identify the wear mechanisms and characterize the tribofilms formed on the wear marks.
- Investigate the interaction between the nanolubricant and the patterned surfaces, understanding how they influence each other through the previously mentioned characterization techniques.

2 LITERATURE REVIEW

2.1 TRIBOLOGY

Tribology is a multidisciplinary field that focuses on the study of friction, wear, and lubrication of interacting surfaces in relative motion. The increase interest in studying tribology has occurred since the second industrial revolution because of the big economic impact of the components that failed due to wear (JOST, 1996).

The definition of the three terms that define the study of tribology are as it follows: Friction is the force that resists the motion of objects in contact, occurring when two surfaces come into contact and experience resistance as they slide against each other. Wear, on the other hand, refers to the gradual deterioration of materials due to repeated frictional forces. Lastly, Lubrication involves the use of lubricants to minimize friction and wear between interacting surfaces (JEYAPRAKASH; YANG, 2021).

The study of wear aims to understand the underlying mechanisms, predict the lifespan of materials, and develop strategies to mitigate wear-related issues. The underlying wear mechanism are of extreme importance to understand the tribological system, it is important to point out that different wear mechanism usually occur simultaneously, they include:

- Abrasive wear: occurs when hard particles or surface asperities cause progressive wear as they come into contact and slide against another surface.
- Adhesive wear: occurs when there is a transfer of material between the moving surfaces, leading to the formation of adhesive or adhesive wear. This occurs especially under high pressures and temperatures.
- Fatigue wear: occurs when surfaces are subjected to repetitive loading and unloading cycles, resulting in cracks, fractures, and progressive material failure.
- Tribochemical wear: occurs when chemical reactions take place between the contacting surfaces during frictional motion. The interaction between the surfaces leads to the formation of chemical compounds or surface layers that contribute to the wear process (JEYAPRAKASH; YANG, 2021).

The formation of tribofilms, in particular, is a characteristic of tribochemical wear. Tribofilms are thin, protective layers that develop on the surfaces during sliding. They can be composed of reaction products between the contacting surfaces or may result from the decomposition or reaction of lubricants or additives present in the system. They can either

mitigate wear with their possible lubrication and protect the surfaces from further wear or increase wear, depending on their composition, thickness, and adhesion to the surfaces (ZUM GAHR, 2010).

Calculating wear and determining wear rates are essential in evaluating the performance and reliability of components. Wear rate is typically quantified by measuring the material loss or volume change over a specific period and sliding distance.

2.2 PATTERN

Since the early 20th century, researchers have been exploring the influence of surface finishes in mechanical applications. The concept of surface patterning was first introduced in the 1940s to reduce friction in honing technology (COBLAS et al., 2015). However, it wasn't until the past three decades that patterning technology gained more interest firstly due to its potential in reducing friction in tribological systems (ROSENKRANZ et al., 2021), then for biological and optical applications.

Surface patterning refers to the modification of a surface without altering its chemical composition, with the aim of creating structured arrays with specific parameters such as shape, arrangement, and size to meet application requirements (FARIA et al., 2020). Surface patterning can be performed at both micro and nano scales. Figure 1 displays different types of fabricated surface texturing. There are some widely employed pattern parameters to define the pattern, including pattern geometry (e.g., micro-dimple, micro-grooves, nano-dots, micro-pits, micro-pillars, and inverted pyramids), pattern size, pattern depth, and pattern area density (VISHNOI et al., 2021).

Figure 1 - SEM images of different types of fabricated surface patterning: (a) square (protrusion), (b) semi hemispherical (recessed), (c) grooves (recessed), (d) hexagon (protrusion), (e) rectangle (recessed) and (f) triangle (recessed).

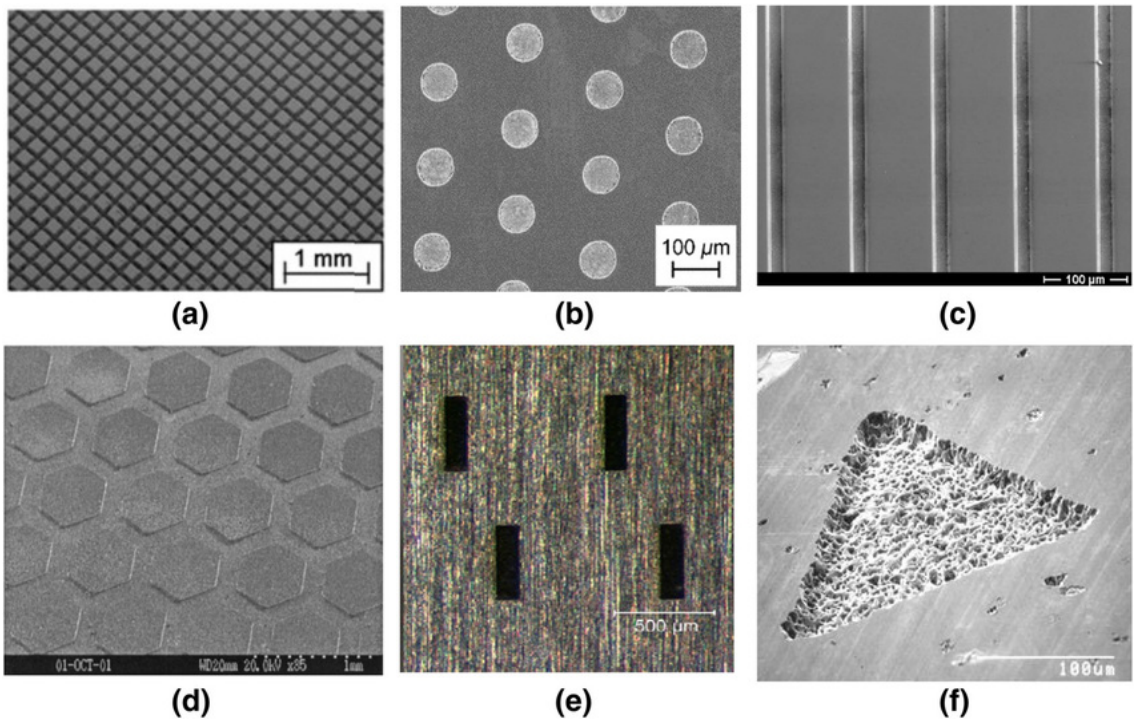

Source: Ibatan; Uddin; Chowdhury (2015).

2.2.1 Surface Patterning Fabrication Techniques

Patterns can be obtained through the following methods:

- Adding material: the pattern features are created by adding material to the surface, usually patterned coatings.
- Removing material: the pattern features are created by removing material from surface, creating micro or nanoscale depressions. In this study, a material removal technique will be used.
- Moving material: the pattern features are due to plastic deformation and redistribution of material.
- Self-forming: wear-resistant regions are formed on a surface through wear, resulting in a pattern in which the wear-resistant regions remain above the surrounding material (COBLAS et al., 2015; BRUZZONE et al., 2008).

Table 1 provides an overview of various fabrication techniques for producing textures through material removal, each with its own advantages and limitations. The technique chosen depends on factors such as the desired texture parameters, the material being textured, and the intended application.

Table 1 – Fabrication Techniques to obtain Texturization through Removing Material.

Type of Material Removal	**Material Removal Method**	**Fabrication technique**
Thermal removal	Laser methods	Lasertext (LT)
		Masked excimer laser
		Laser honing
		CNC focused lasers
	Electrical discharge machining (EDM)	Electrical discharge texturing (EDT)
	Electrical beam texturing	
	Ion beam texturing (IBT)	
Chemical etching	Masking methods	Chemical texturing
		Electrochemical texturing
	Non-masking methods	Self-assembling
		Maskless laser assisted etching
		Maskless electrochemical texturing
		Anisotropic etching
Mechanical	Machining with defined geometry tools	CNC ultrasonic machining
		Mechanical honing
		Microcutting
	Machining with non-defined geometry tools	Grinding
		Free abrasive machining
		Patterned erosion

Source: Adapted from Bruozzone et al. (2008).

Among the available techniques, laser surface texturing is the most frequently used technique. It involves the removal of material through an ablation process (VENCL et al.,

2019). It is a low-cost process, easy to operate with precise control of the shape of the texture, and large area processing (BISWAS et al., 2019; OBILOR et al., 2022; PETTERSSON et al, 2007; TALA-IGHIL et al, 2011). However, some laser fabrication methods present some drawbacks, such as possible modification of the microstructure of the material due to excessive heating (known as heat affected zone) affecting the quality of the samples, increased time as compared to other techniques as the machining speed is low, and the smallest pattern features possible to obtain are typically between 10 to 50 μm due to the wavelength-specific diffraction limit (VISHNOI; KUMAR; MURTAZA, 2021; ZHANG et al., 2023; AGUILAR-MORALES et al., 2018).

In this study, dry plasma etching induced by ion bombardment is employed as the fabrication technique. It offers great potential for scalability, allowing multiple samples to be processed simultaneously, and it does not produce a heat-affected zone like laser ablation methods. However, this technique is not commonly used for transition metals, as their low vapor pressure makes efficient etching challenging. Additionally, a mask is employed to obtain the desired patterns, and finding a mask that remains intact during the etching process can be challenging (LE DAIN et al., 2021).

Dry and wet plasma etching are the most often employed techniques in the electronics industry, particularly in circuit board manufacturing, as they allow the replication of tightly controlled micron-sizen and nano-sized features (GENG, 2005). A representation of the texturing obtained in dry etching of mc-Si wafers used in electronics industry is shown in Figure 2.

Figure 2 - SEM images of mc-Si wafers textured by (a) masked dry plasma etching, (b) mask-less dry plasma etching using Cl2 plasma and (c) metal catalyst assisted mask-less dry plasma etching using SF6 /O2 plasma.

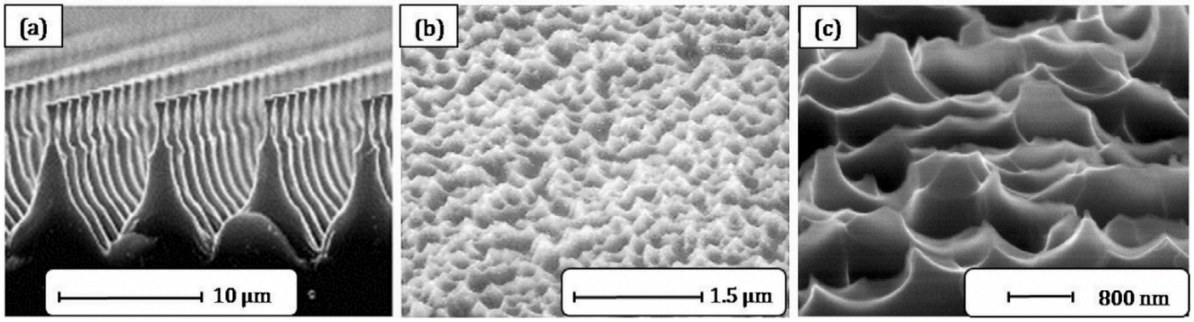

Source: Adapted from Sreejith et al. (2022).

Dry etching selectively removes material from a substrate through sputtering caused by highly energetic species present in the plasma. This process involves the use of a plasma reactor, typically a reactive ion etching (RIE) or inductively coupled plasma (ICP) reactor, where a low-pressure gas is excited to a plasma state. The substrate to be etched is placed in the plasma reactor and biased, attracting high-energy ions that bombard the surface, resulting in physical sputtering and chemical reactions that lead to material removal from the substrate (MANOS; FLAMM, 1989). The ICP reactor configuration typically used for this process is shown in Figure 3.

Figure 3 – ICP reactor configuration.

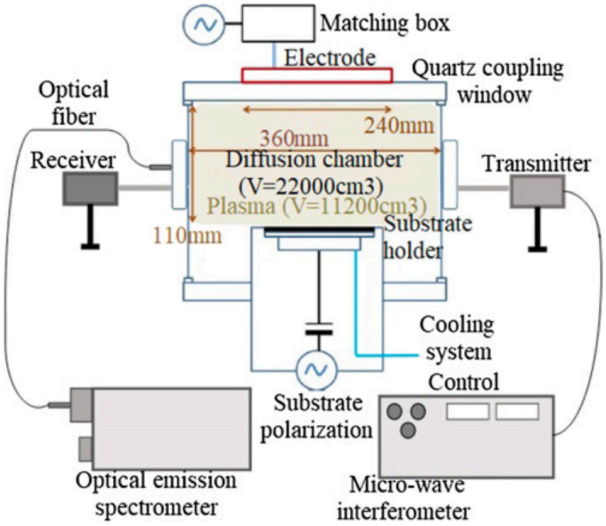

Source: Adapted from Le Dain et al. (2021).

Halogen-based plasmas, such as chlorine (Cl) and fluorine (F) plasmas, are commonly utilized in dry etching processes for electronic silicon-based devices and can also be applied to metals due to their adequate etch rates. However, caution must be taken as halogen atoms or molecules can remain on the etched material's surface, leading to potential corrosion issues, besides the handling of these gases must be approached with great care, as they pose significant risks to the environment and human health.

In an effort to address these concerns, researchers have explored the use of organic plasma mixtures, which present a lesser threat. For instance, pure ion bombardment or the formation of volatile organometallic compounds can enable the etching of certain metals using plasma mixtures like methane (CH_4) or propionaldehyde (C_3H_6O). However, maintaining plasma stability can be challenging in such cases, and the breakdown of organic compounds

may result in the deposition of carbonaceous material in the plasma source (ORLAND; BLUMENTHAL, 2005; LE DAIN et al., 2021).

In this context, Le Dain et al (2021) studied the dry plasma etching of pure iron (Fe), pure chromium (Cr), and Fe-Cr alloys with chromium contents ranging from 1-12 % wt, since chromium and iron are the main elements of stainless steel. For etching pure iron and chromium, they used pure chlorine gas and pure argon gas, the results obtained are shown in Table 2. As expected, chlorine gas (Cl_2) exhibited the highest etching rate in relation to argon gas (Ar), etching iron was more efficient than etching chromium due to the formation of iron chloride ($FeCl_3$), a volatile compound that is adsorbed in iron surface (process known as chemical etching), and the subsequent ion bombardment facilitates the desorption of this compound. However, chromium does not exhibit such high etching rates because the temperature is too low to form chromium volatile compounds, therefore for chromium the etching mechanism is mainly occurring by sputtering. When etching Fe-Cr alloys, only Cl_2 gas was used, the study found that the etching rate significantly decreased with increasing chromium content, with rates of 244, 129, and 67 nm/min observed for 0, 3, and 12% wt of Cr, respectively. This is attributed to the formation of hard zones around Fe sites caused by the presence of Cr sites, contributing to the decrease in etch rate as well as decrease in desorption probabilities (LE DAIN et al., 2021).

Table 2 – Etching rates (nm/min) using pure Cl_2 gas and pure Argon gas.

Sample	Cl_2	Ar
Fe	269 (±5)	40 (±1)
Cr	45 (±3)	26 (±2)

Source: Le Dain et al (2021).

2.2.2 Tribological Behavior of Patterned Surfaces

Regarding the tribological performance of patterned components, they have shown significant potential in reducing friction and wear. The main mechanisms behind these improvements are the entrapment of wear debris within the textures and lower contact area between the friction pairs. The entrapment of wear debris prevents their presence at the sliding

interface, while the decrease in contact area ensures that a smaller portion of the surface is exposed to wear.

Considering these benefits, Rosenkranz et al. have summarized the main design guidelines found in literature, which are summarized below. These guidelines aim to provide proper guidance and precautions when utilizing patterned surfaces in dry sliding conditions, with the ultimate goal of enhancing tribological performance (ROSENKRANZ et al., 2021).

Spacing of Patterns: When the distance between pattern features is too large, it may hinder the efficient entrapment of wear debris, potentially leading to debris agglomeration and ploughing.

Surface Pattern Area Coverage: Excessive surface pattern area coverage may decrease the availability of smooth regions capable of bearing the normal load, thereby reducing load-carrying capacity.

Pattern Depth: Deep pattern features can result in edge stresses that induce excessive plastic deformation.

Pattern Size: Patterns must be designed to accommodate the largest wear debris effectively.

Residual Stresses: Selecting a proper surface patterning technique that reduces the generation of residual stresses is crucial.

Indirect Effects: Understanding how surface patterns can influence properties that indirectly affect friction and wear, such as heat transfer and surface energy, is imperative.

Rationally Designed Textures: Patterns designed with a clear rationale, especially those informed by simulations, can be harnessed to enhance overall tribological performance.

Combining Texturing with Solid Lubricants: A pivotal consideration is the potential synergy between surface texturing and solid lubricants. While surface texturing alone can reduce ploughing and adhesion components of friction in dry conditions, the possibility of further reducing these components when combined with solid lubricants poses intriguing questions. Design guidelines for these combined approaches will depend on the specific characteristics of the solid lubricant and the extent to which patterning affects its structural and chemical properties (ROSENKRANZ et al., 2021).

2.3 LUBRICATION

Lubrication plays a fundamental role in various industries as it can significantly reduce costs. Implementing proper lubrication practices ensures that equipment operates efficiently, leading to reduced energy consumption and extended component lifespan.

The concept of lubrication involves minimizing friction and wear between surfaces that are in relative motion by employing a lubricant. A lubricant is a material with a lower shear strength than the surfaces it comes in contact with. The aim is to form a lubricant layer either in the form of a liquid, solid, or gas with a low shear strength. The lubricant layer reduces the contact between surface irregularities, therefore reducing resistance to movement and minimizing friction and wear (QIU et al, 2017).

The far most used types of lubricants are liquid or grease lubricant but under extreme conditions like high or low temperatures, vacuum, or radiation, liquid lubricants may not be effective (ERDEMIR, 2001). To address this challenge, the application of solid lubricants becomes necessary. Table 3 presents a synthesis of different extreme conditions where using liquid lubricant may be challenging, and advantages of using solid lubricants in these conditions.

Table 3 – Comparison in terms of applications of Solid and Liquid Lubricants in Tribological Applications.

Application Environment and/or Condition	Solid Lubricants	Liquid and Grease Lubricants
Vacuum	Some solids (i.e., transition-metal dichalcogenides) lubricate extremely well in high vacuum, have very low vapor pressure	Most liquids evaporate, but perfluoropolyalkylethers (PFPE) and polyalfaolefins (PAO) have good durability
Pressure	Can endure extreme pressures	May not support extreme pressures without additives
Temperature	Relatively insensitive; can function at very low and high temperatures; low heat generation due to shear	May solidify at low temperatures and decompose or oxidize at high temperatures; heat generation varies with viscosity
Electrical conductivity	Some provide excellent electrical conductivity	Mostly insulating
Radiation	Relatively insensitive to nuclear radiation	May degrade or decompose over time
Wear	Provide excellent wear performance or durability at slow speeds and under fretting conditions; lifetime is determined by lubricant film thickness and wear rate	Provide marginal performance and durability at slow speeds and under fretting conditions; need additives for boundary lubrication
Friction	Extremely low friction coefficients are feasible	Depends on viscosity, boundary films, and temperature
Thermal conductivity and heat dissipation capability	Excellent for metallic lubricants; poor for most inorganic or layered solids	Good
Storage	Can be stored for very long times (dichalcogenides are sensitive to humidity and oxygen)	May evaporate, drain, creep, or migrate during storage
Hygiene	Better industrial hygiene due to little or no hazardous emissions; since they are in solid state, there is no danger of spillage that can contaminate environment	May release hazardous emissions; liquid lubricants may spill or drip and contaminate environment; fire hazard with certain oils and greases
Compatibility with tribological surfaces	Compatible with hard-to-lubricate surfaces (i.e., Al, Ti, stainless steels, and ceramics)	Not suitable for use on non-ferrous or ceramic surfaces
Resistance to aqueous and chemically aggressive environments	Relatively insensitive to aqueous environments, chemical solvents, fuels, certain acids and bases	May be affected or altered by acidic and other aqueous environments

Adapted from Erdemir (2000).

2.3.1 Solid Lubrication

There are different types of solid lubricants such as layer-lattice solids, soft solids, polymeric films (BRITANNICA, 2020). Most solid lubricants exhibit lubrication due to their lamellar or layered crystal structure (ERDEMIR, 2001), which are characterized by weak bonding forces between the layers, resulting in a low shear strength. The shear strength differs in different directions as the bond energy of the atoms within each layer is much larger than Van der Walls interactions between the layers of the structure (STACHOWIAK; BATCHELOR, 2005). Consequently, the layers of these materials align parallel to the direction

of relative motion and move smoothly over each other, facilitating efficient lubrication (MIYOSHI, 2001).

2.3.2.1 Carbon Derived from Carbide (CDC) Structure, Fabrication Techniques and Tribological Behavior

One type of layered solid lubricant is the Carbon Derived from Carbide (CDC) which is the result of the remotion of metallic or non-metallic atoms from a carbide structure, like Silicon Carbide (SiC), Titanium Carbide (TiC), Vanadium Carbide (VC), and Boron Carbide (B_4C). This process can originate many different forms of carbon, ranging from highly amorphous to highly crystalline structures (PRESSER et al, 2011), depending mainly on the temperature that the process is carried out. When CDCs are synthesized at a temperature under 1000 °C, they tend to be highly amorphous with a mixture sp^2 and sp^3 hybridization, however, as the temperature increases and approaches the graphitization temperature, CDCs tend to have a more organized and structured arrangement, showing a higher proportion of sp^2 hybridization (URBONAITE; HÄLLDAHL; SVENSSON, 2008). It is worth mentioning that obtaining CDCs is more energy efficient than obtaining graphite as the graphitizing is close to 3000 °C (MARSH; RODRÍGUEZ-REINOSO, 2006).

The fabrication technique mostly commonly known to obtain CDCs is a synthesis reaction using gases like chlorine or fluorine, although is a time efficient process is highly toxic and corrosive. Besides, CDCs remain bonded to its precursor material in this process, therefore limiting its versatility and application (WANG; SHAO, 2016; SUI; LU, 2011).

To address these limitations, an alternative method for CDCs production have been developed, which relies on solid-solid reactions. This method offers advantages in terms of safety and cost-effectiveness. However, it is important to acknowledge that there is limited research available on this approach (NEVES, 2020).

Neves (2020) achieved a highly efficient solid-solid reaction, producing CDCs, specifically nanocrystalline carbon with 2D turbostratic lamellar structure, as observed in the SEM images presented in Figure 4 and the Raman spectrum characteristic of a turbostratic structure shown in Figure 5. The reaction consisted of chromium carbide (Cr_3C_2) and boron carbide (B_4C) as precursors, subjected to a synthesis reaction carried out at 1300 °C,

subsequently a chemical extraction was employed and then it was obtained practically all the carbon present in the system (NEVES, 2020).

Figure 4 – SEM Images of 2D Turbostratic Graphite obtained from solid-solid reaction between Cr_3C_2 and B_4C.

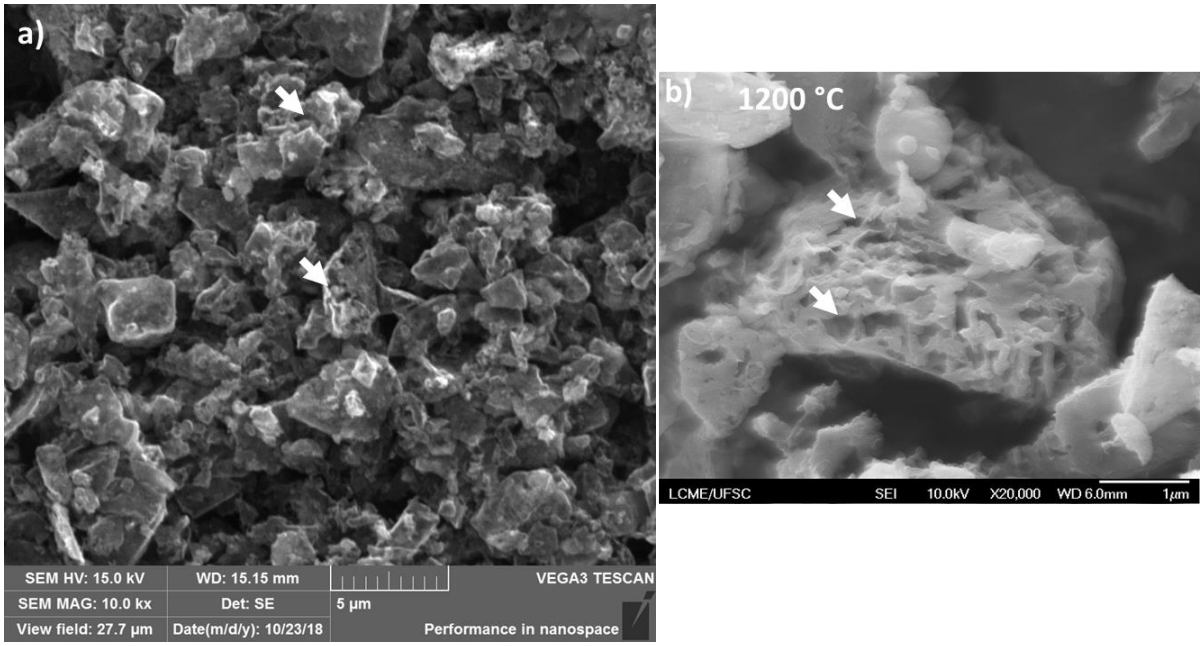

Source: Neves (2020).

Figure 5 – Raman Spectroscopy of 2D Turbostratic Graphite obtained from solid-solid reaction between Cr_3C_2 and B_4C. (a) First-order bands from Raman Spectroscopy. (b) Second-order bands from Raman Spectroscopy.

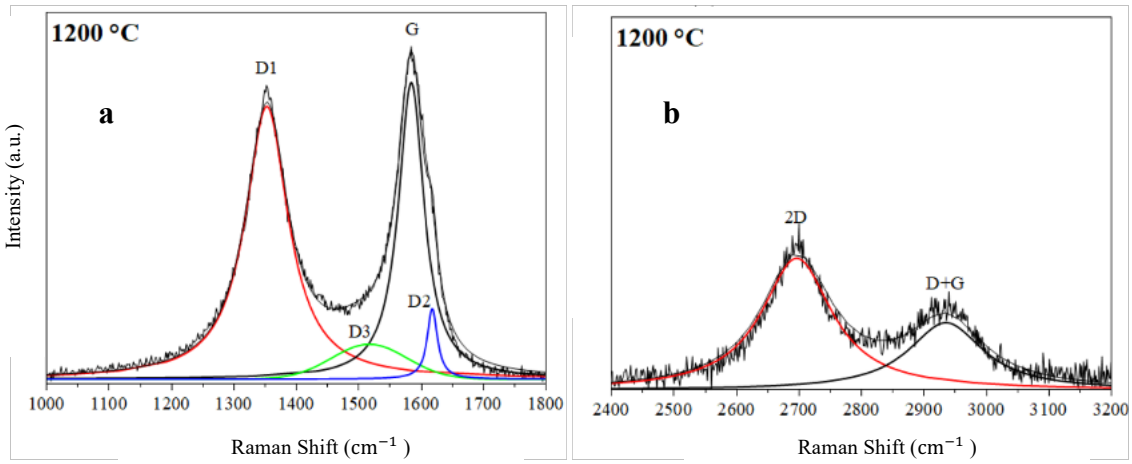

Source: Neves (2020).

The CDC structure obtained on this solid-solid reaction, 2D turbostratic graphite, is highly disordered with a mixture of sp^2 and sp^3 hybridization. 2D turbostratic graphite demonstrates excellent tribological behavior, with a friction coefficient (COF) of 0.07 and a wear rate that is 70% lower compared to 3D graphite under the same conditions (NEVES, 2020). The gradient of mechanical properties and strain capacity observed in CDCs facilitates the softening of the surfaces promoting lubricity (PRESSER; HEON; GOGOTSI, 2011).

2.3.1.2 Raman Spectrocopy Characterization Technique

Raman spectroscopy is often utilized to characterize the changes to the chemical composition and structural changes of the crystal lattices of carbon.

The Raman Spectroscopy is a technique that involves illuminating a sample with a laser, its principles are based on identifying molecular interactions resulted from the shifted scattered light, most of the scattered light has the same energy (wavelength) as the incident laser light (Rayleigh scattering). However, a small fraction of the scattered light undergoes a change in energy due to interactions with molecular vibrations or rotations. This shifted light is known as Raman scattering and it contains information about the molecular vibrations in the sample. The resulting spectrum, called a Raman spectrum, displays peaks that correspond to the vibrational frequencies of the molecules in the sample. Each peak represents a specific type of molecular bond or vibration (KUMAR, 2012).

The bands in Raman spectra provide information about the material's crystal lattice. The first order bands for carbon materials adjusted by Lorentzian function are given in the range between 1300 cm^{-1} and 1600 cm^{-1}, as an example, the first-order bands of carbon materials, including the 2D turbostratic graphite are shown in Figure 6. The G band, which usually occurs at around 1580 cm^{-1}, is associated with the in-plane vibration of sp^2-hybridized carbon atoms and is indicative of the highly ordered hexagonal lattice structure. On the other hand, the D band, appearing at approximately 1350 cm^{-1}, is associated with structural defects or disorder within the carbon material, such as the presence of grain boundaries or edge defects. It is worth noting that the intensity of D band divided by intensity of G band (I_D/I_G) is widely utilized as a measurement of the carbon structure disorder (REICH; THOMSEN, 2004). Another parameter also widely used is Full Width at Half Maximum (FWHM) which describes the width of a peak

or curve at half of its maximum height or intensity, in this case the FWHM of the D band is a form to quantify the disorder (JORIO et al., 2011).

Figure 6 – Raman Spectra First-order Bands. (a) Carbon derived Cr_3C_2-B_4C sintered at 1200 °C, (b) 2D graphite derived from Fe-SiC e (c) 3D mineral graphite.

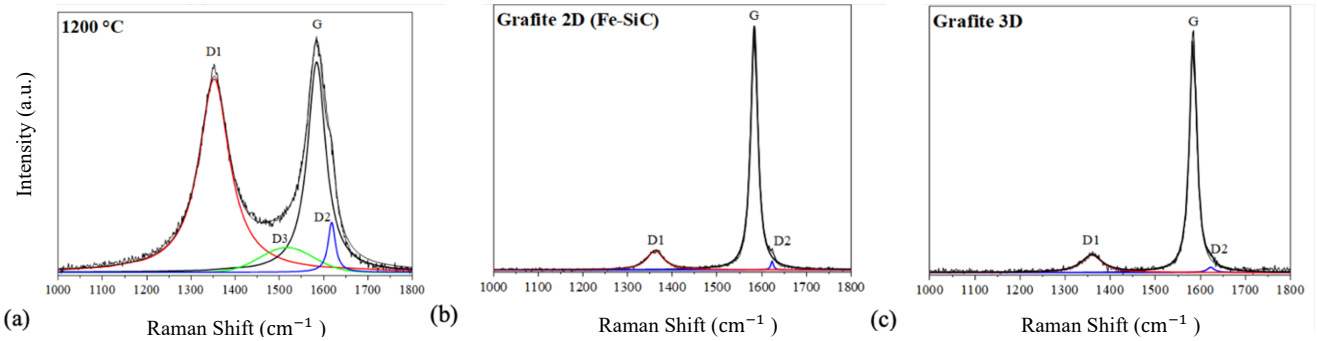

Source: Neves (2020).

Furthermore, the deconvolution of these bands, which is a step that involves separating overlapping peaks in the Raman spectrum, may show the presence D2 and D3 bands in carbon materials as also indicated in Figure 6. D2 band, typically at 1620 cm^{-1}, also indicates point defects in the material (PIMENTA et al., 2007). While D3 band, typically at 1520 cm^{-1}, indicates an amorphous portion in the material therefore graphite doesn't present this band (SADEZKY et al., 2005).

Regarding the second-order bands that by Lorentzian function are given typically in the range 2500 cm^{-1} and 2800 cm^{-1}. The 2D band provides information about graphene stacking order. As shown in

Figure 7, the 3D graphite, which is a more ordered material, is adjusted by two Lorenzian functions while 2D graphite and 2D turbostratic graphite are adjusted only by one function. (FERRARI; ROBERTSON, 2001; JORIO et al., 2011). A way of determining if the carbon is turbostratic is through the FWHM of the 2D band, the FWHM of a single-layer graphene's 2D band is approximately 30 cm^{-1}, values above this indicate the carbon is turbostratic (FERRARI; BASKO, 2013).

Within this spectral range, there are other bands that are typically observed, such as the D+G band at approximately 2950 cm^{-1} and 2*D' at around 3200 cm^{-1}. These bands result from a combination of the D band, which is linked to structural defects and disorder, and the G band, which represents a structurally ordered lattice. Consequently, the presence of these bands

also serves as an indication of material disorder and the presence of defects (PIMENTA et al., 2007).

Figure 7 – Raman Spectra Second-order Bands. (a) Carbon derived Cr_3C_2-B_4Cr sintered at 1200 °C, (b) 2D graphite derived from Fe-SiC e (c) 3D mineral graphite.

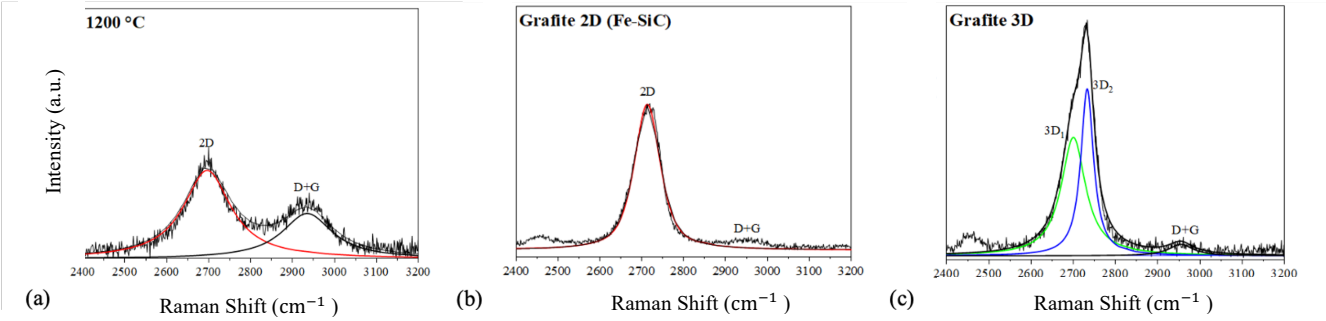

Source: Neves (2020).

2.4 TRIBOLOGICAL BEHAVIOR OF PATTERNED SURFACES FUNCTIONALIZED WITH SOLID LUBRICANTS

There is already great potential in tribological performance of patterned surface and solid lubricant when considered individually as commented on the previous sections. Therefore, the combination of these two technologies may harnesses the benefits of each, resulting in enhanced tribological performance.

There are four distinct scenarios in which surface patterning is combined with solid lubricants, as illustrated in Figure 8. In the first three scenarios, the surface pattern is initially created, and then solid lubricants are deposited into the pattern. In the fourth scenario, a wear-resistant coating is first applied to the surface, followed by the creation of the texture. While case 1, which involves a continuous film over the pattern, is more commonly found in the existing literature, the current study will adopt case 3. In this approach, nanoparticles will be deposited uniformly throughout the entire surface (HUANG et al., 2023).

Figure 8 – Surface Texture combination with solid lubricant Possibilities.

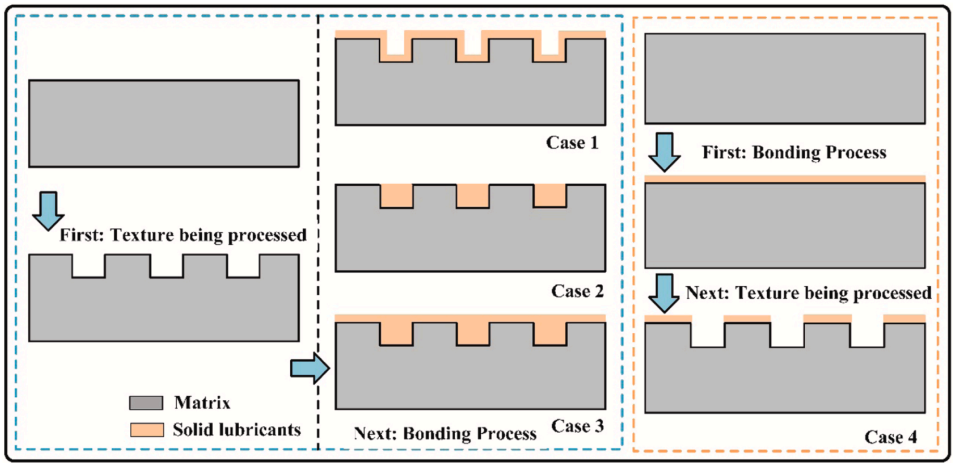

Source: HUANG et al., 2023.

As cited in section 2.2, Rosenkranz et al (2021) provided design guidelines for enhancing the tribological performance of surface patterns in dry conditions. Similarly, Huang et al (2023) proposed design guidelines specifically for patterns with solid lubricants aiming for a synergistic effect between the surface texture and the solid lubricants. These guidelines can be summarized as it follows:

Optimized Surface Texture Parameters: Surface pattern parameters, including shape, geometry, parameters, must be thoughtfully designed. The coverage of surface textures should have a balance, avoiding excessive density that could compromise material bearing capacity while still enabling effective lubrication.

Appropriate Solid Lubricant Selection: The solid lubricants should be chosen by considering the working environment, such as temperature, atmosphere, as well as the specific working parameters (pressure, speed, etc.). Additionally, the selection of solid lubricants should meet the specific tribological property requirements (e.g., coefficient of friction, wear volume, service life), taking into account the material properties of various solid lubricants.

Reasonable Preparation of Multi-Solid Lubricants: When employing multiple solid lubricants or additives to create composite multi-solid lubricants, it is necessary to take into consideration the synergistic effects that may arise between these various lubricants.

Matrix-Solid Lubricant Compatibility: Compatibility between the metal matrix and the solid lubricant must be ensured in order to avoid occurrence of large interface defects and poor

adhesion between the solid lubricant and the matrix, as it can hinder the formation of a complete lubricating film during friction.

Thoughtful Composite Technology Preparation: The tribological properties of solid lubricating materials are directly influenced by the bonding characteristics and release rates of solid lubricants within the surface texture therefore the preparation method for composite technology should be taken into consideration carefully.

Consideration of Indirect Parameters: Indirect parameters that can affect tribological properties, including factors like vibration, noise, heat transfer, and surface energy should be evaluated (HUANG et al., 2023).

Overall, if well designed and functionalized for the tribological system patterned surfaces combined with layered materials offer advantages from both technologies. The surface patterns act as reservoirs, trapping wear debris and reducing the contact area, while the layered materials facilitate sliding. Moreover, studies have shown that the patterned surfaces can store lubricants and transfer it to the untextured regions during sliding. Additionally, the mechanical engagement of the layered material in the textures can improve its adhesion to the substrate, promoting better stability and performance (RAPOPORT et al., 2008; ZHANG et al., 2017; ROSENKRANZ et al., 2021).

Regarding the solid lubricant types utilized in combination with the patterns, MoS_2 is the most commonly found layered lubricant in literature. Comparisons between different layered materials on textured surfaces have shown that both graphite and MoS_2 outperform calcium fluoride (CaF_2) and hexagonal boron nitride (hBN). However, comparisons between MoS_2 and graphite are inconclusive, which may be associated to the tribological performance of these lubricant in different environment conditions (MENG et al., 2019; SONG et al., 2019; WANG et al., 2020 ROSENKRANZ et al., 2021).

The initial size of solid lubricant particles before application to the texture has also been studied. Nanoscale MoS_2 or graphite particles have shown lower friction compared to the same material deposited in the form of microscale particles (HUA et al., 2016; WANG et al., 2020; ROSENKRANZ et al., 2021).

Regarding the pattern shape, grooves and dimples are the most commonly used texture features in combination with layered materials. Other shapes like rectangles, squares, and triangles have been explored but have not shown superior performance (CHEN et al, 2018; SEGU et al., 2013; ROSENKRANZ et al., 2021).

The optimization of pattern density has been the focus in some patterns with layered material studies. Most of these studies have shown that pattern density is the main parameter affecting the most friction, wear, and durability. However, the optimal pattern density varies widely across studies. This may be explained as the area density of the pattern increases there are more reservoirs to store lubricant, however as the pattern density becomes excessive, it causes an increase in surface roughness and decreases the area of the surface available to support contact stresses and resist abrasive wear. Therefore, it is likely that the studies demonstrate different results as they usually cover a part of the range of the area density then depending on if they are closer to a rougher surface or not, they will present worsening tribological performance with increasing area density or enhancement (RIPOLL et al., 2013; VOEVODIN et al., 2006).

3 EXPERIMENTAL PROCEDURE

Figure 9 illustrates the experimental procedure of this study, indicating the processing and characterization steps.

Figure 9 - Synthesis of the Experimental Procedure.

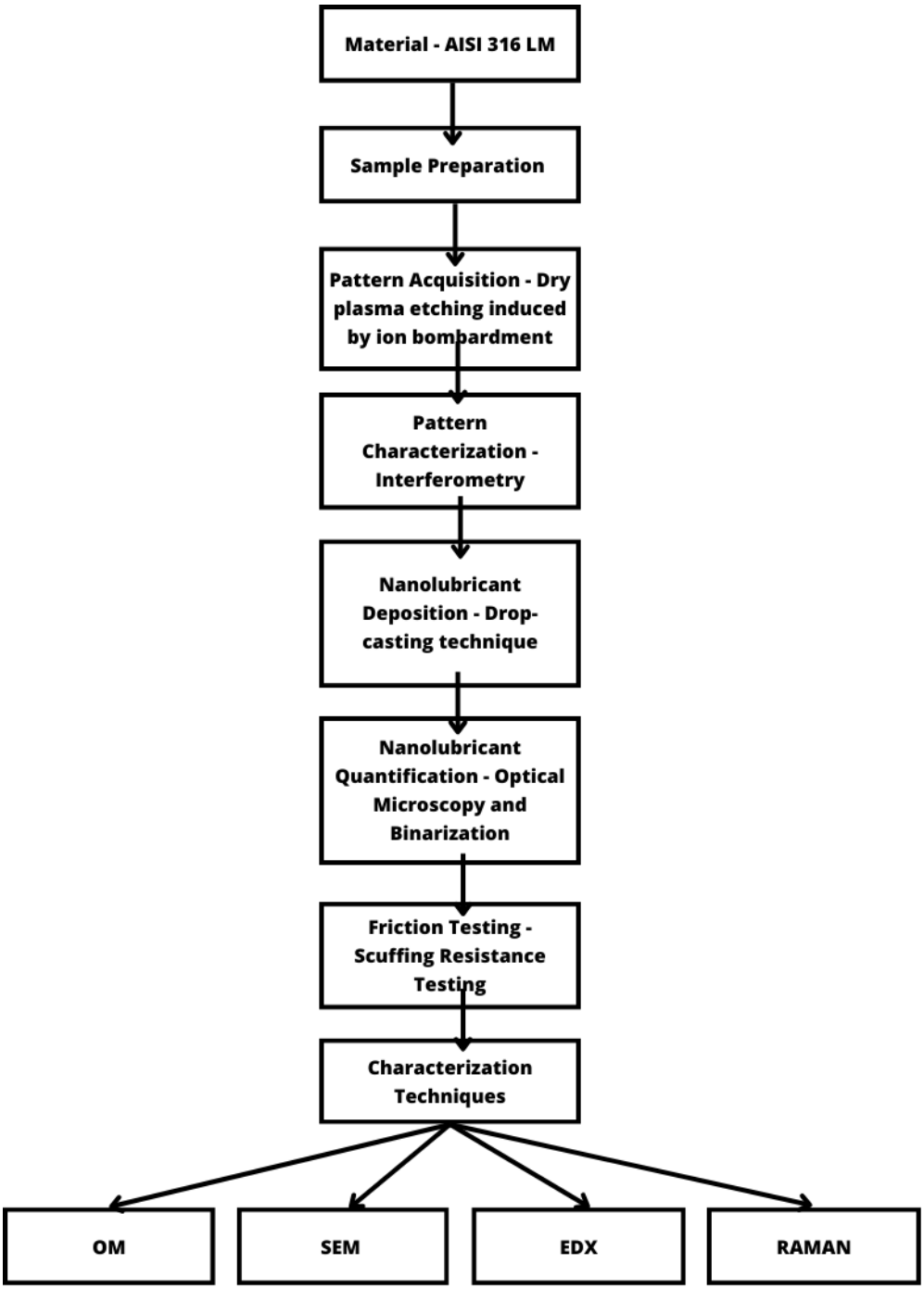

Source: Own authorship.

3.1 MATERIALS

The material utilized in this study was an austenitic stainless steel AISI 316 LM, with a composition according to ASTM standards (17 wt% Cr, 13 wt% Ni, 2 wt% Mo, 0.5 wt% Si, 0.2 wt% Mn and 0.02 wt% C). The samples were cut to a height of 3 mm and had a diameter of 20 mm. The surface of the samples was prepared through a polishing procedure, using a series of SiC abrasive papers with progressively finer grit sizes up to mesh 4800, followed by a final polishing step utilizing polishing clothes and a diamond abrasive spray with particles measuring three microns and subsequently one micron, resulting in a mirror-like finish. To ensure sample cleanliness, the polished samples were immersed in ethanol and placed on an ultrasonic bath for 10 minutes before being dried for further analysis.

3.2 SURFACE PATTERNING

After completing the polishing and cleaning steps, the samples were subjected to surface patterning. In this study, a material removal fabrication technique was employed to create patterns on the surface. The patterns were obtained using dry plasma etching induced by ion bombardment. The patterning processes, as detailed in the subsequent sections 3.2.1 and 3.2.2 were carried out by the research team Plasmas – Procédés – Surfaces, at Institut Jean Lamour (IJL) and the research team in Institut des Matériaux de Nantes Jean Rouxel (IMN), respectively. More information on patterning technologies performed on this study can be found in the following cited studies (PAVLIK et al., 2020; LE DAIN et al., 2021).

The samples were labeled according to their texture parameters: H for height, which indicates the depth of the dimples; D for diameter, which refers to the diameter of the dimples; and A for area density of the pattern, which represents the surface percentage covered by the dimples. For instance, the label H2-D100-A4 denotes a pattern with dimples that are 2 micrometers (μm) in height, 100 μm in diameter, and cover 4% of the surface. Therefore, a total of 5 conditions, which the surface parameters are detailed in Table 4, were investigated in this study: a mirror-polished surface designated as MPS (used as a reference sample), the large dimples pattern group: H2-D100-A4, H2-D100-A15, and the small dimples pattern group: H0.8-D9-A30, and H0.6-D9-A40.

Table 4 – Pattern Parameters of the Surfaces utilized in this study.

Classification	Surface Identification	H (depth of the dimples, µm)	D (diameter of the dimples, µm)	A (area density of the pattern, %)
Mirror-polished surface	MPS	-	-	-
Small Dimples Pattern	H0.8-D9-A30	0.8	9	30
	H0.6-D9-A40	0.6	9	40
Large Dimples Pattern	H2-D100-A4	2	100	4
	H2-D100-A15	2	100	15

Source: Own authorship.

3.2.1 Dry plasma etching induced by ion bombardment fabrication process carried out to obtain the large dimples patterns

For surface patterning of the samples H2-D100-A4 and H2-D100-A15, a Multi-Dipolar Electron Cyclotron Resonance (MDECR) plasma reactor was used along with a direct current bias (DC) bias. This plasma reactor utilizes microwave energy to generate a plasma discharge, while a magnetic field is applied to sustain and direct the plasma, the multi-dipolar configuration of the magnetic field allows a more efficient ionization of the gas, resulting in a highly reactive plasma capable of etching the material on the sample surface. The configuration MDECR plasma reactor consists of a vacuum chamber, an antenna, a magnetic field generator, and a gas inlet system.

Furthermore, the introduction of a DC bias to the cathode where the samples are placed enhances the ion bombardment on the surface and increases the etching rate. Since the negative potential on the cathode attracts the positive ions in the plasma towards the surface, causing them to collide and remove material from the sample.

The procedure to achieve the desired patterns on the samples, as illustrated in Figure 10, can be outlined as follows: Firstly, in order to obtain a mask to transfer the pattern into the samples, a thin stainless-steel sheet with a thickness of approximately 250 µm was drilled using a laser, incorporating the desired texture shape and associated parameters. Subsequently, the

samples were covered with the drilled stainless steel, and positioned on a substrate holder inside the MDCER plasma reactor chamber (PAVLIK et al., 2020).

Figure 10 – Large Dimples Pattern Fabrication Process.

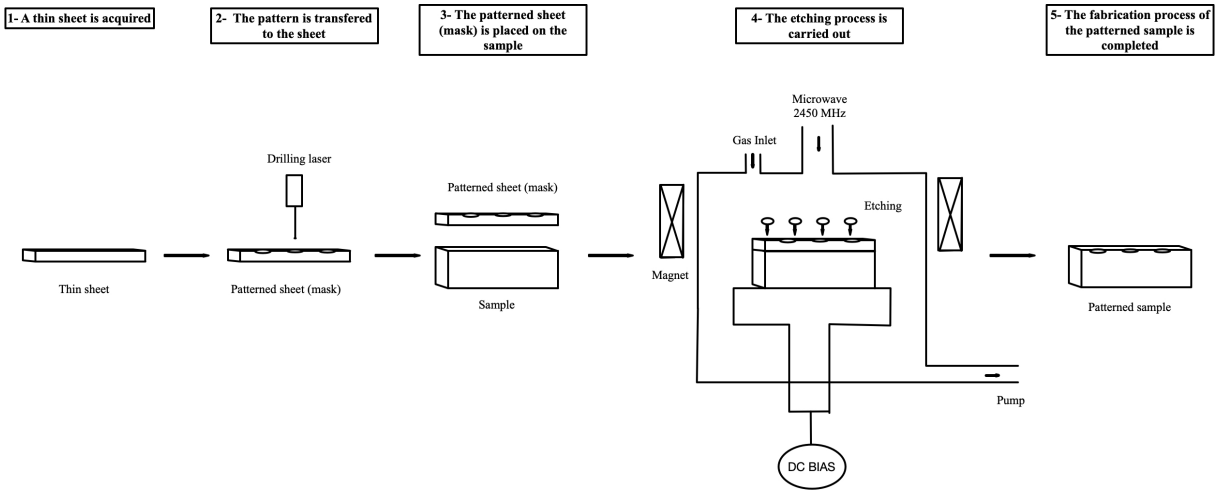

Source: Own authorship.

Therefore, the etching cycle was initiated. Vacuum was established at approximately 10^{-4} Pa, and the plasma was generated using a mixture of 95% argon (Ar) and 5% hydrogen (H_2) gas at a pressure of 2.5 Pa with a substrate bias of -400 V. The patterning cycle was carried out for 150 minutes (PAVLIK et al., 2020).

3.2.2 Dry plasma etching induced by ion bombardment fabrication process carried out to obtain the small dimples patterns

The surface patterning of the samples H0.8-D9-A30, and H0.6-D9-A40 was performed in an Inductively Coupled Plasma (ICP) plasma reactor. The ICP reactor operates by employing a high-frequency radiofrequency (RF) power supply to ionize the gas and initiate the plasma state. The plasma generated in the ICP reactor exhibits excellent plasma uniformity and high electron density. The ICP reactor configuration consists of vacuum chamber, RF antenna, gas inlet system, and additionally a DC bias was also employed to enhance the ion bombardment to the cathode and consequently the etching rate (CONRADS; SCHMIDT, 2000).

To obtain the patterns, firstly the samples were masked with a SiO_2 layer using Plasma-Enhanced Chemical Vapor Deposition (PECVD), a technique that deposits thin films by utilizing plasma. The SiO_2 layer had a thickness of around 500 μm. Then, the samples were patterned using optical lithography, a method commonly used in semiconductor manufacturing

that uses light to transfer a pattern from a mask to a photosensitive material. Thirdly the etching step was performed in the plasma reactor previously mentioned accordingly the following etch conditions, 100% Cl_2 gas at a pressure of 0.66 Pa with a substrate bias of -150 V. Following the etching step, the remaining SiO_2 masks were removed using SF_6/CHF_3 plasma within the same reactor (LE DAIN et al., 2021). A schematic representation of the outlined fabrication process is illustrated in Figure 11.

Figure 11 – Small Dimples Pattern Fabrication Process.

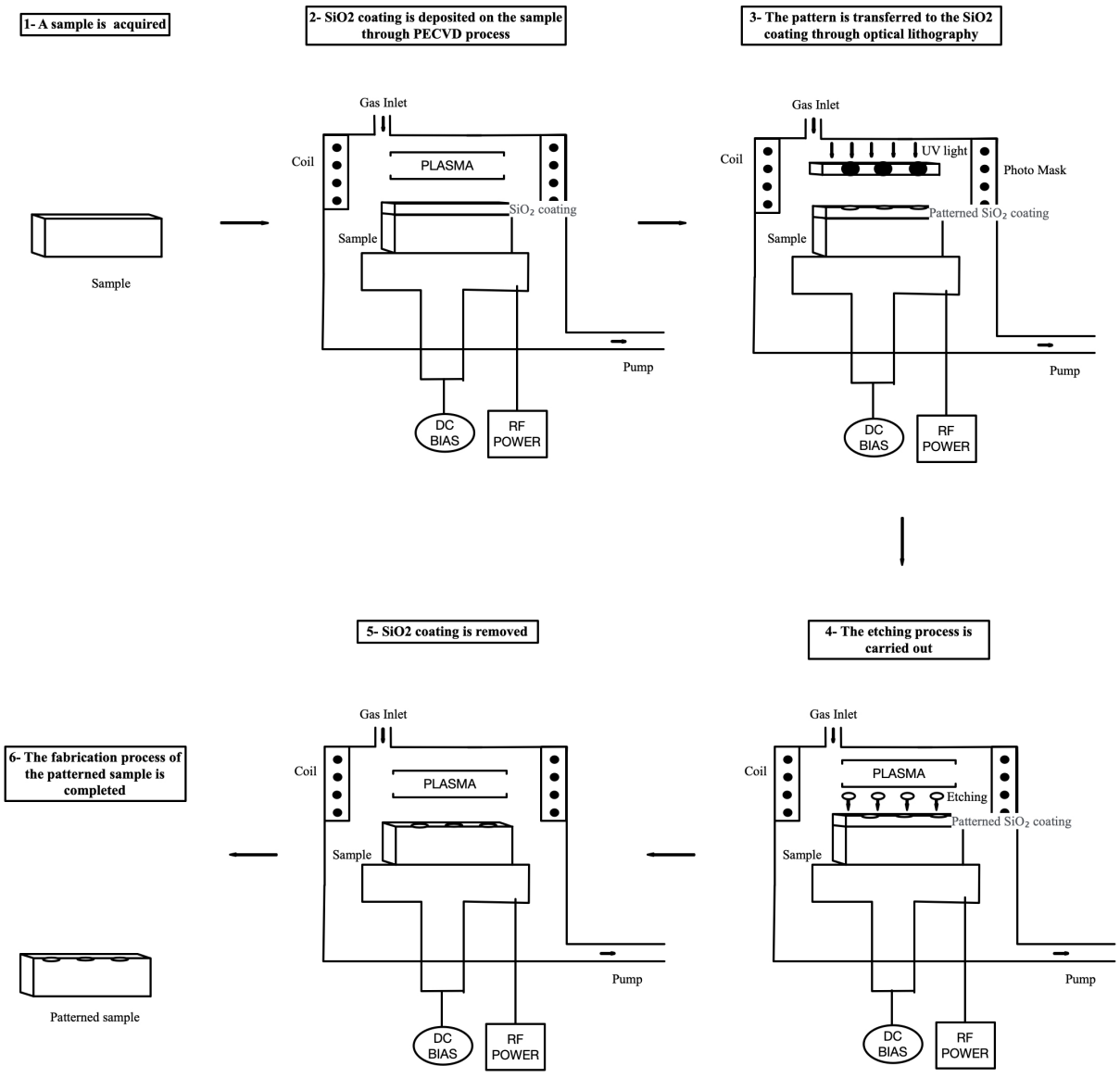

Source: Own authorship.

3.3 NANOLUBRICANT DEPOSITION: DROPCASTING

The selection of the deposition method was based on Giacomelli's study, which aimed to improve repeatability and minimize waste of nanolubricant by comparing spin coating and drop-casting techniques. Giacomelli experimented with three solvents (ethanol, isopropanol, and acetone) and two solid nanolubricants: 2D turbostratic graphite (CDC) or graphene particles, varying the number of solution applications. He found that the drop-casting technique resulted in higher repeatability and required a lower quantity of nanolubricant. Besides, the combination of isopropanol and 2D turbostratic graphite resulted in a more homogeneous distribution and a smaller coffee ring effect compared to other solvent and nanolubricant combinations. The coffee ring effect refers to the phenomenon where a liquid evaporates on a solid surface, leaving a ring-like structure due to the non-uniform evaporation rate and the particles move towards the edge of the material's surface, it is important to control this effect to obtain a uniform distribution of nanolubricant. Further information about this technique and results obtained can be found in Giacomelli's thesis (GIACOMELLI, 2020).

Therefore, based in his study, isopropanol solvent and 0.05% wt of 2D turbostratic graphite was used. The nanolubricant was dispersed in the solvent by subjecting the suspension to sonication for a total of 2 minutes and 30 seconds, alternating between 30 seconds of sonication and 30 seconds of rest to prevent excessive heating.

The deposition was carried out in a room with controlled relative humidity and temperature of 40-50% and 23°C, respectively. Prior to the deposition process, the samples were ultrasonically cleaned with acetone for 10 minutes, followed by ethanol for another 10 minutes and then dried in warm air.

A precision micropipette (Labmate PRO, 100 µl capacity) was employed to deposit the nanolubricant. An amount of 4 µl/cm² of suspension was applied per application, resulting in a total of 20 µl per application on the 25 mm diameter samples.

Figure 12 illustrates the deposition process. For the first application, on the image is illustrated by letter "a", a circular movement was made on the imaginary circumference between the center and the extremity of the sample. It is essential to ensure that there is a droplet at the end of the micropipette throughout the entire movement, and the user must maintain a consistent velocity while applying the suspension, being careful not to touch the surface of the sample. For subsequent applications, a drop was applied to the center of each quadrant of a circle, on the image this step is illustrated by letter "c". A time interval of 2 minutes and 30 seconds was given between applications to allow the solvent to evaporate and ensure even distribution.

Figure 12 – Deposition Sequence of 2D turbostratic graphite

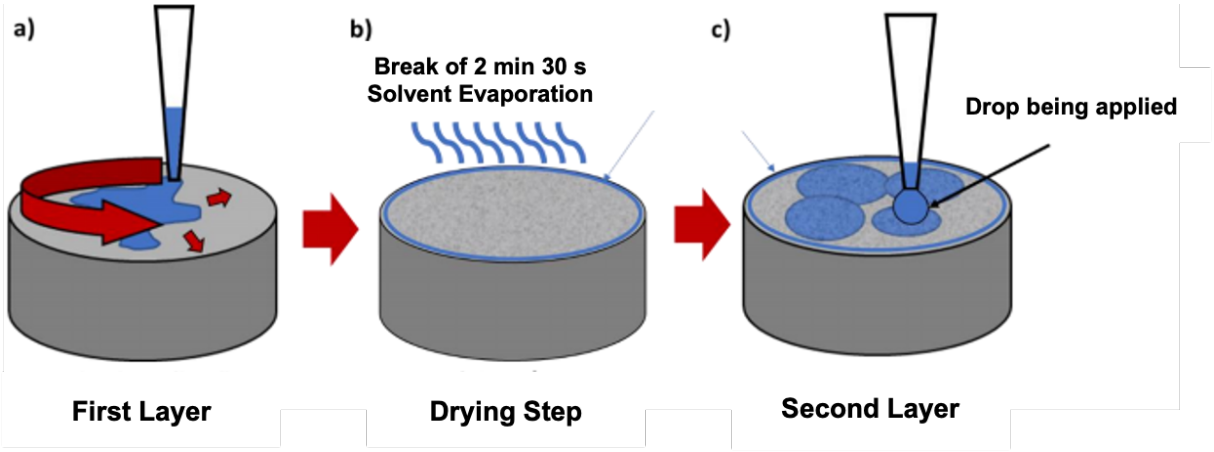

Adapted from (GIACOMELLI, 2020).

3.4 SURFACE CHARACTERIZATION

To gain a comprehensive understanding of the pattern parameters, the amount of lubricant, tribological behavior, wear mechanisms, and compositional changes occurred during the wear mechanisms, a range of techniques were employed to characterize the sample surfaces.

3.4.1 Optical interferometry

Optical interferometry was used to characterize the pattern parameters, such as depth, diameter, spacing, and area coverage of the dimples. The Zygo Newview 7300 white light optical interferometer was employed to capture 3D maps of the surface being analyzed with a precision of 0.1 nm in the normal direction to the surface and a lateral resolution of up to 0.276 µm for the maximum equipment magnification. The procedure for data acquisition involved one acquisition of 1 mm² area for each surface condition from this study using the objective lense 20x.

Further, data analysis was performed using MountainsMap® 7.4 analysis software from the manufacturer Digital Surf. To obtain the pattern parameters through this software, the following steps were taken: firstly, a horizontal profile passing through the center of the dimples was extracted. Followed by the utilization of the step profile tool to determine the height and width of the pattern element. Subsequently, the profile distance measurement tool was applied to determine the distance between the pattern elements. Additionally, to determine the pattern

area coverage, the image was first converted into a binary format using the binary threshold operator, and then the study from the software “statistics on all grains” was employed to determine the area density of the pattern. It is worth noting that data analysis was performed without using filters, as the objective was to obtain information about the shape (waviness) of the pattern parameters, rather than the roughness.

3.4.1 Optical microscopy

Optical microscopy was utilized for the following purposes to characterize if nanolubricant dispersion was homogeneous, the nanolubricant area coverage, the size of the agglomerates, and to evaluate the wear mechanisms following scuffing resistance testing. Micrographs were obtained using Leica DM4000/DFC450 reflected light optical microscope.

Nanolubricant amount was a fundamental factor to ensure that the lubricant concentration was consistent across all samples and did not affect the tribological test results, therefore the images were acquired through the optical microscope then binarized through the software ImageJ. The following steps, were followed to acquire the nanolubricant area coverage: (i) micrographs of the mirror-polished sections of all samples were obtained at 200x magnification, (ii) the images were cropped to a rectangular shape until the scale bar, with dimensions of 352 x 230 millimeters, (iii) brightness and contrast were adjusted to highlight the particles, , (iv) the images were transformed into 256 shades of gray by choosing the 8-bit option under the type tab, (v) the Non-Local Means Denoising filter was utilized to remove noise (RASBAND, 1997-2014), (vi) the Unsharp Mask filter was applied to enhance the edges, (vi) The median filter was applied to eliminate any isolated noise, (viii) the image was binarized using the threshold, and (ix) the area percentage of the particles was measured. Figure 8 shows the effects resulting from the application of the aforementioned filters.

Figure 13 – Nanolubricant Area Coverage Procedure. (a) Initial micrograph at 200x magnification. (b) Image after brightness and contrast adjustments. (c) Transformation of the image into an 8-bit format. (d) Application of the Non-Local Means Denoising filter. (e) Application of the Unsharp Mask filter. (f) Application of the of the median filter. (g) Binarization of the image, resulting in 31.42% nanoparticles area coverage.

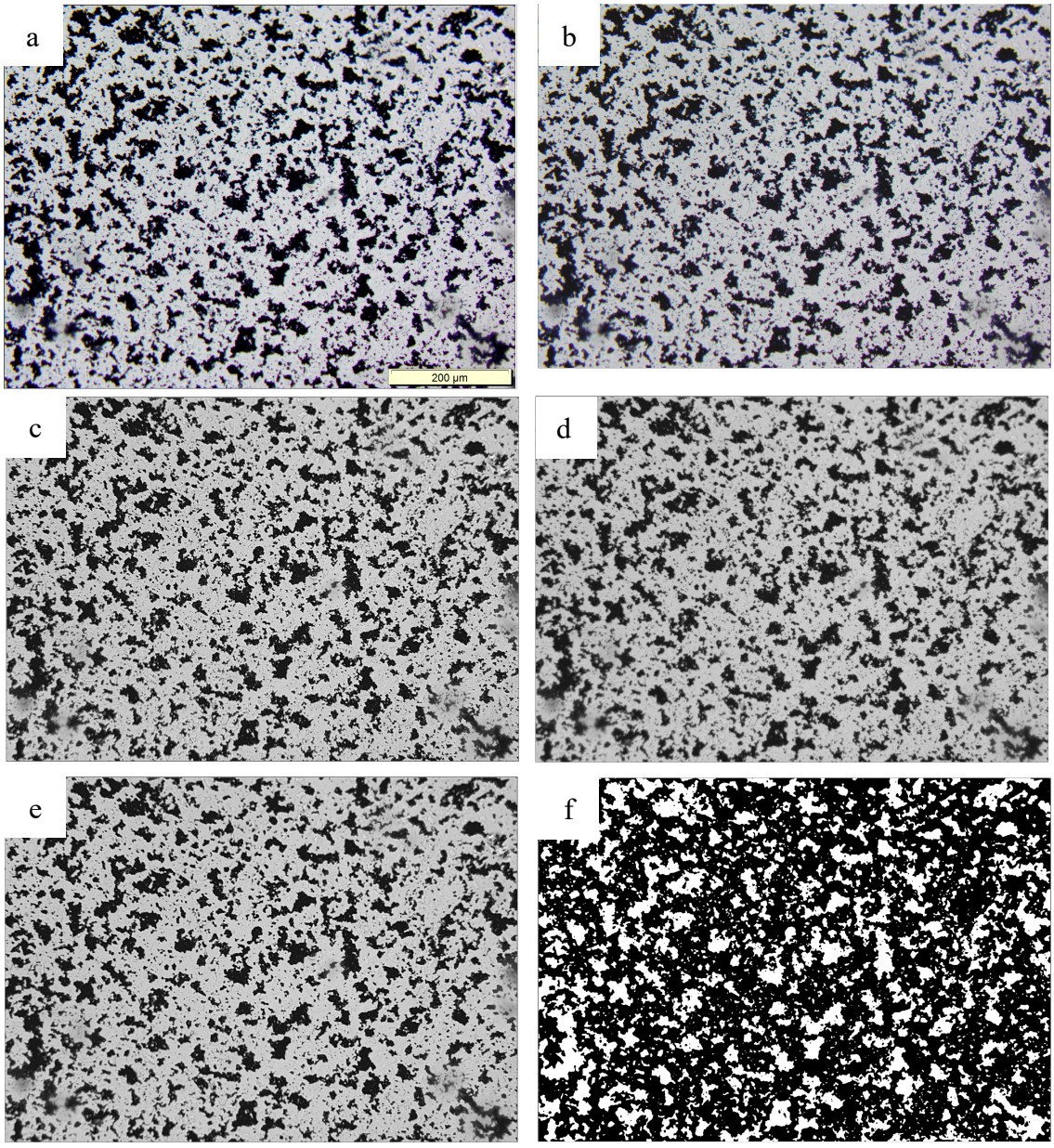

Source: Own authorship.

Furthermore, to determine the size of the particles and gain insights into their disposition within the patterns, the following steps were taken after quantifying the nanolubricant area coverage: the scale in the ImageJ software was calibrated, and afterwards the line and measuring tools were employed to obtain the size of the agglomerates in their major axis.

3.4.2 Tribology

To evaluate the tribological performance of the patterned samples with solid lubricant deposition, scuffing resistance testing was carried out.

The scuffing resistance testing was performed using the methodology developed by De Mello and Binder (2006). This method compares different materials in terms of their ability to maintain lubricity, as measured by their durability. The testing process involves applying incremental loads at fixed time intervals (10 min) until the material is no longer at the self-lubricating regime, meaning the friction coefficient overcome 0.2. The durability is calculated by multiplying the maximum load that the sample withstood until the friction coefficient (COF) reached 0.2 by the maximum sliding distance that the sample withstood. Besides the full-length scuffing resistance testing, which it was just described, interrupted scuffing resistance testing was also conducted specifically at the 8-minute mark during the second incremental load.

The obtained data from the scuffing resistance testing were represented in a graph, as an example is shown a graph from this study in Figure 14. The graph presents various elements that provide valuable information about the tribological responses of the samples under investigation.

One of the displayed elements is the load line (Fz), which indicates the incremental load applied during the test. This line shows how the load increases over time, providing information about the load-carrying capacity of the material.

The friction coefficient (COF) line is another important feature in the graph. It demonstrates the frictional behavior of the sample as it slides against counterpart's surface. In the lubricity regime, the COF line remains below 0.2, in this graph is possible to observe that the sample remained in the lubricity regime until the third load, indicating effective lubrication. However, once the COF reaches 0.2, it means that the material is no longer in the lubricity regime, and the test ends at this point. At this moment is already possible to determine the

durability by multiplying the maximum sliding distance (value in x-axis) by the maximum applied load (value in y-axis) within the lubricity regime.

Additionally, the graph includes the contact electrical resistance line (R), which offers insights into the tribological behavior. Changes in the electrical resistance can be correlated with variations in surface contact and the formation or degradation of a tribofilm. In this study, it was observed that as a tribofilm formed, the electrical resistance increased. Conversely, when the COF starts to arise, indicating the loss of lubricity, the tribofilm deteriorated or underwent changes in its chemical composition, resulting in a decrease in electrical resistance, as observed in Figure 14.

Figure 14 – Representative Graph of a Scuffing Resistance Testing.

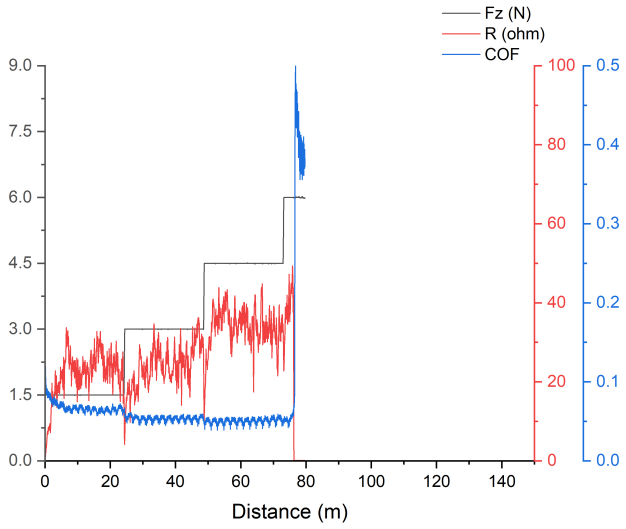

Source: Own authorship.

The scuffing resistance testing was performed using a CETR UMT-2 tribometer with a reciprocating sliding motion under ambient conditions at 23 °C and a relative humidity between 40% and 50%. The testing parameters used in the study are presented in Table 5. Additionally, it is important to note that it was employed a load cell with a 10 N capacity for the testing. For this reason, the testing conditions were established such that the samples could withstand a maximum load of 9 N, resulting in a maximum attainable durability of 1314 N·m.

Table 5 - Parameters of Scuffing Resistance Testing.

Parameters of Scuffing Resistance Testing	
Type of Testing	Reciprocating
Diameter 52100 steel sphere	5 mm
Size of the track	5 mm
Load (by increments)	1.5 N
Interval of the loads	10 min
Frequency	4 Hz

Source: Own authorship.

3.4.3 Scanning Electron Microscopy (SEM) and Energy Dispersive X-ray Spectroscopy (EDX)

The images obtained by SEM analysis provided detailed information regarding the morphology of the wear tracks, debris particles, and lubricant deposition, allowing a better comprehension of the wear mechanisms involved in the tribological performance of the samples.

Additionally, EDX characterization enabled the identification of elements present in the samples, contributing to a better understanding of the composition and possible changes caused by the friction tests.

TESCAN VEGA3 LMU Scanning Electron Microscopy with a tungsten filament was employed for this analysis. The instrument was able to acquire high-resolution images with high magnifications using both secondary electron (SE) and backscattered electron (BSE) detectors. The SE imaging provided qualitative details of the surface, and the BSE imaging offered insights into the compositional variations. In addition, the microscope was equipped with an Oxford EDX microprobe, allowing the chemical analysis of the samples.

3.4.4 Raman Spectroscopy

The Raman Spectroscopy was utilized to identify changes to the chemical composition and structural changes of the crystal lattices of carbon (nanoparticles) due to wear, being essential to evaluate the wear mechanisms after the scuffing resistance testing.

The laser needs to be carefully chosen to analyze the specific lattices structures. In this study, a laser wavelength utilized was aimed to identify the oxide and carbon bands. The experimental setup involved using a Renishaw InVia model 2000 equipped with an argon laser operating at a wavelength of 514.5 nm. Raman spectra were acquired with a 10-second acquisition time in the range of 200 to 3500 cm-1, with 3 accumulations per measurement.

4 RESULTS AND DISCUSSION

This section will present the results obtained from this study and discussion about them. Firstly, the topography characterization will be discussed to present the pattern characteristics. Secondly, the deposition of the nanolubricant will be evaluated to determine its uniformity and distribution across the different samples. Thirdly, the tribological response of the samples will be evaluated through quantifiable results such as durability, friction coefficient, allowing to evaluate their effectiveness in reducing wear and friction. Lastly, wear mechanism characterizations will be discussed to comprehend the reasons for the tribological responses observed, identifying the predominant wear mechanisms observed during the scuffing resistance tests, in addition to understanding how patterning and the solid nanolubricant influence on the wear mechanisms.

4.1 PATTERN TOPOGRAPHY

Five surface conditions were utilized in this study: Mirror-Polished Finish, H0.6-D9-A30, H0.8-D9-A30, H2-D100-A4, and H2-D100-A15, their axonometric projection obtained by optical interferometry is shown Figure 10. It is important to note that in the course of the second production batch of the large dimples samples group, the plasma parameters varied slightly due to the instability of the plasma, resulting in a minor height variation, as shown in Figure 10 “e”, “f”, “h”. However, this variation did not have any impact to the extent of this study and, therefore, was not considered in the analysis.

Figure 15 – Axonometric projection of the surfaces. (a) Mirror Polished Finish. (b) H0.6-D9-A40 pattern. (c) H0.8-D9-A30 pattern. (d) H2-D100-A4 pattern. (e) H3-D100-A4 pattern. (f) H4-D100-A4 pattern. (g) H2-D100-A15 pattern. (h) H5-D100-A15 pattern.

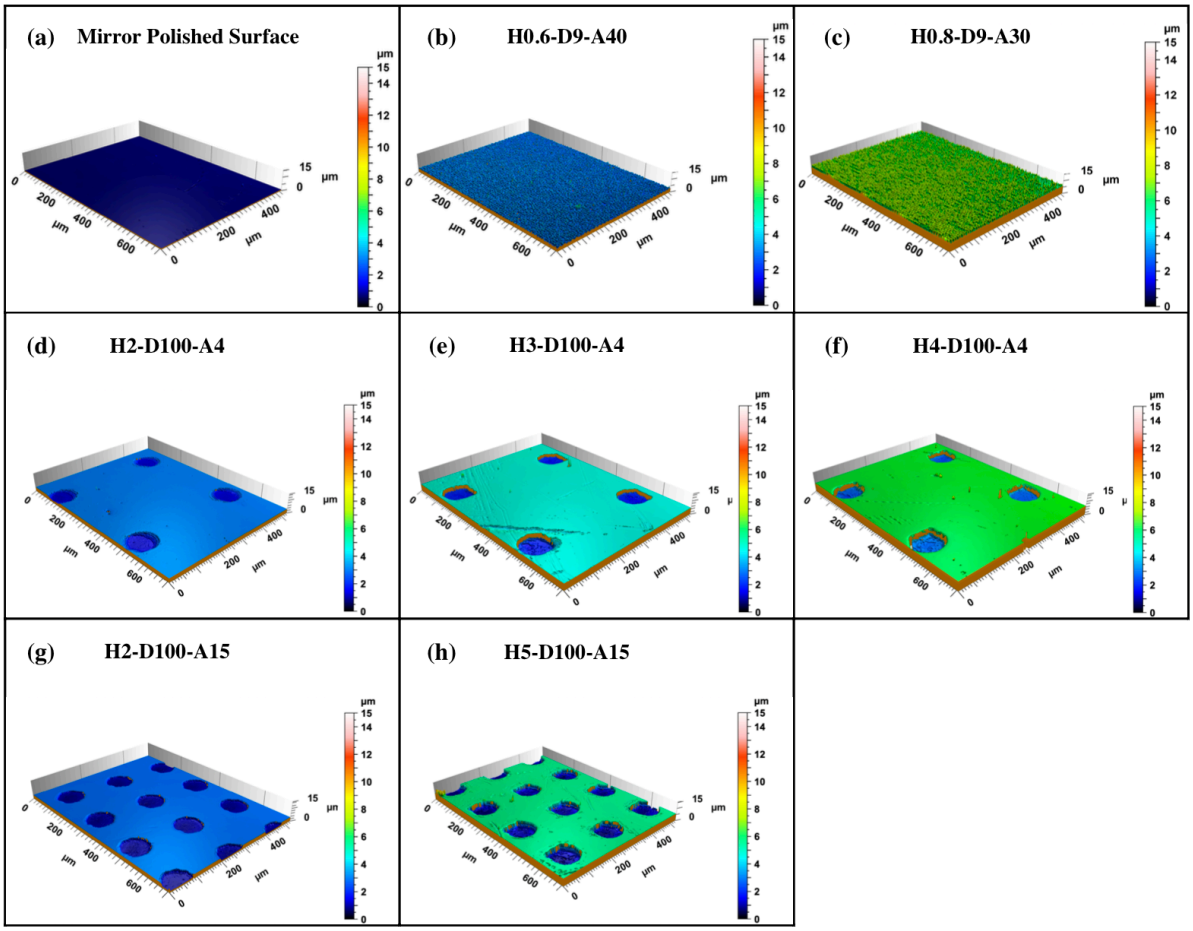

Source: Own authorship.

4.2 NANOLUBRICANT DEPOSITION

Following the deposition of the nanolubricant through the drop-casting technique, images of the polished section of the patterned samples were acquired using the optical microscope and scanning electron microscope. The primary objective of this step was to verify that all samples exhibited a consistent and uniform distribution of the solid lubricant.

Quantifying lubricant within the dimples sections would lead to less reliable results. As the dimples on the samples' surfaces introduce variability due to their uneven pattern. In contrast, the polished surface provides a more stable surface. Consequently, by focusing on examining the polished sections from the patterned samples, the objective was to eliminate

potential biases and achieve greater accuracy in measuring and analyzing the overall lubricant particle distribution across the samples.

Before all tribological behavior trials, except for the first trial, the nanolubricant amount on the polished section of the five samples was measured. The average nanolubricant area coverage was found to be 31.04%, with a standard deviation of 2.47%. To illustrate this process, Figure 11 showcases an example of micrograph along with its corresponding binarization.

Figure 16 – Representative image of the binarization process, on the left is shown the original micrography (a) and on the right the image after the binarization process (b).

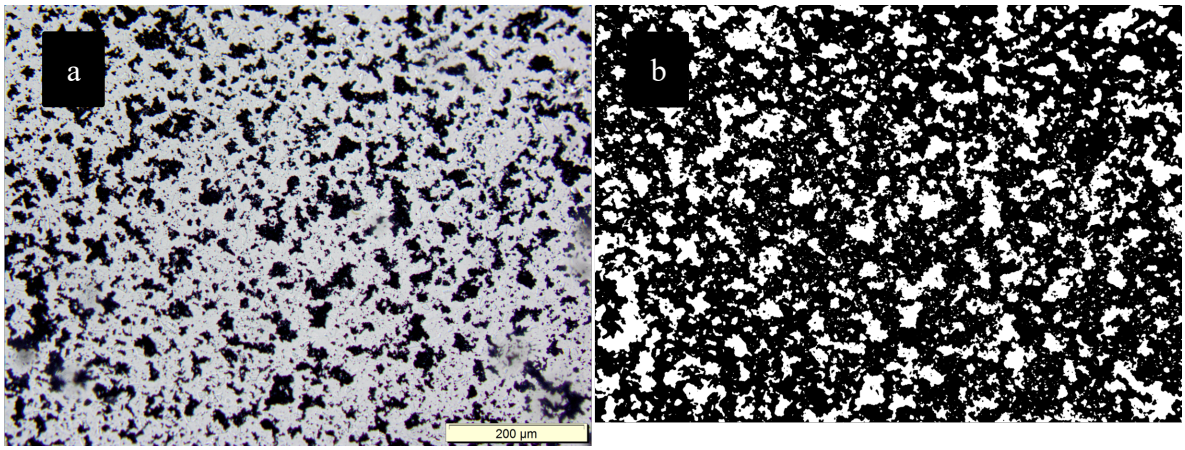

Source: Own authorship

Furthermore, the drop-casting technique employed in this study also facilitated an even and uniform distribution of the lubricant, as demonstrated in the SEM image shown in Figure 12 and in the previous Figure.

Figure 17 – Micrography obtained through SEM of the polished section after the nanolubricant deposition.

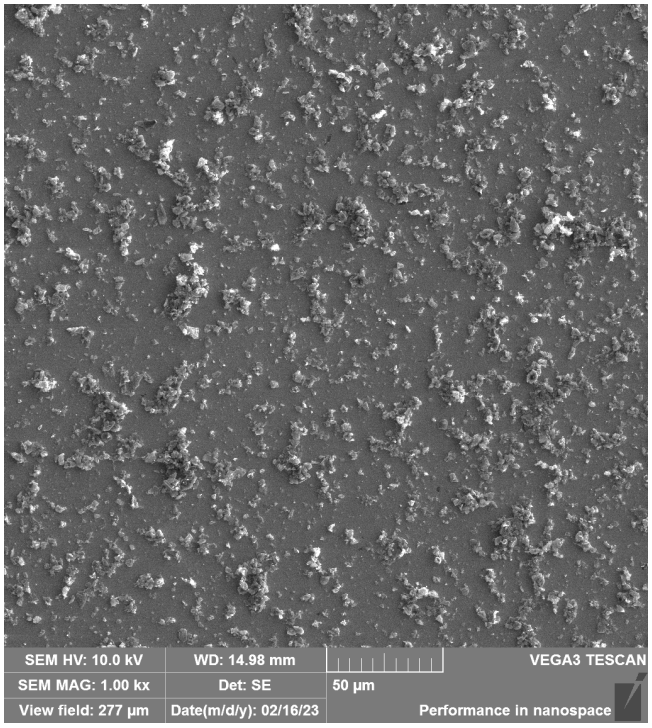

Source: Own authorship.

In the studies conducted by Giacomelli (2020) and Neves (2020) both measured the diameter of nanolubricant particles using CILAS, obtaining average particle diameters of 1.29 and 1.85, respectively. However, due to the method of particle deposition employed in this study involving a solution, these nanoparticles tend to accumulate forming particles agglomerates, as noticed in the previous figures.

The average size of these agglomerates, specifically their major axis, was quantified using ImageJ software, revealing an average value of 46.83 with a standard deviation of 21.57.

To better understand the relationship between the size of solid lubricant particles and surface patterns, two schematic representations for the large dimples pattern group and small dimples pattern group are provided in Figure 13 and Figure 15, along with its corresponding micrographs in Figure 14 and in Figure 16. Figure 13 and Figure 15, along with its corresponding micrographs in Figure 14 and in Figure 16.

In the case of large dimples in Figure 13 and Figure 14, it's evident that the agglomerates tend to occupy the interior of the dimples as they are smaller than the patterns elements. According to the schema, during the sliding motion in the scuffing resistance testing

performed, they tend to be swept to the dimples' interior and as the testing progress and pattern wears down, these agglomerates are gradually released, contributing to lubrication.

Figure 18 – Schematic Representation of the H2-D100-A15 pattern with nanolubricant agglomerates representation.

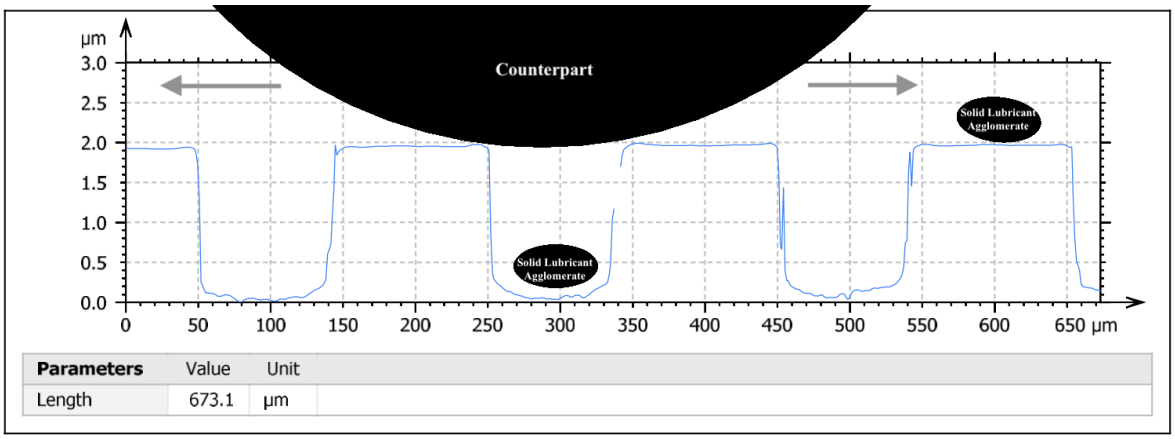

Source: Own authorship.

Figure 19 – Micrography obtained through optical microscopy of the H0.8-D9-A30 pattern after the nanolubricant deposition.

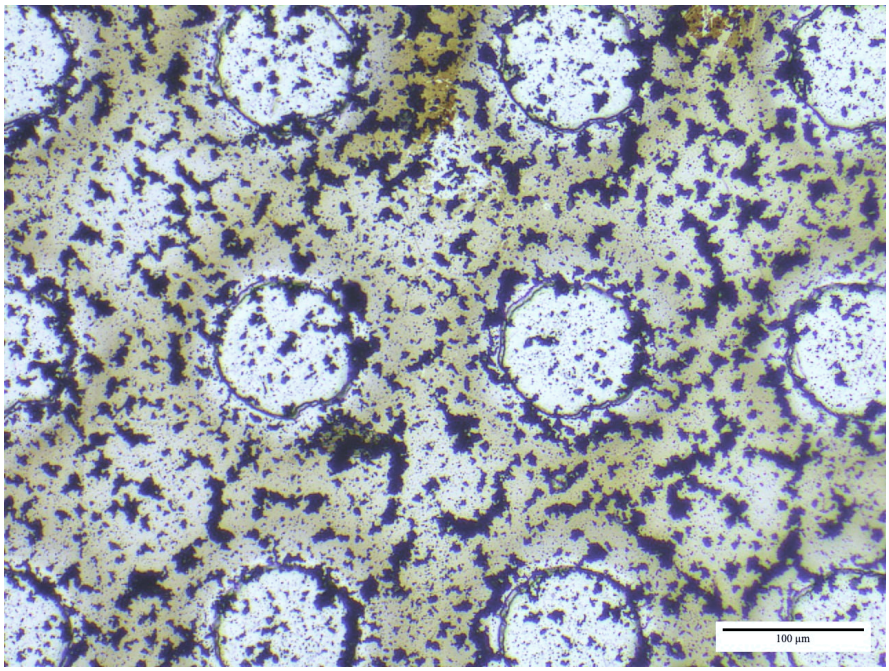

Source: Own authorship.

Conversely, for small dimples, which a schematic representation is shown in Figure 15 and its corresponding micrograph in Figure 16, the agglomerates are larger than the dimples themselves. Consequently, they remain in a continuous contact with the tribological system throughout the test, and as the CDC particles shear, they likely anchor them within the dimples.

Figure 20 – Schematic Representation of the H0.8-D9-A30 pattern with nanolubricant agglomerates representation.

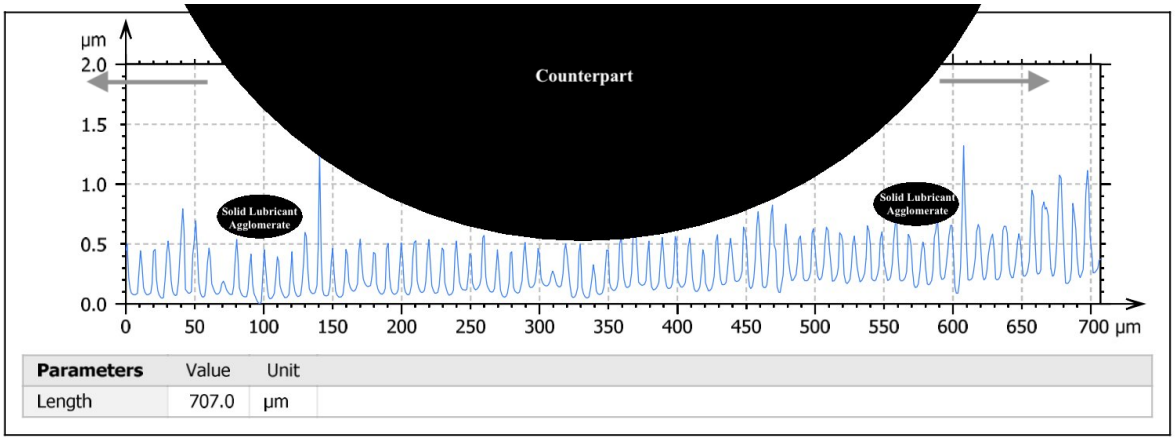

Source: Own authorship.

Figure 21 – Micrography obtained through optical microscopy of the H2-D100-A15 pattern after the nanolubricant deposition.

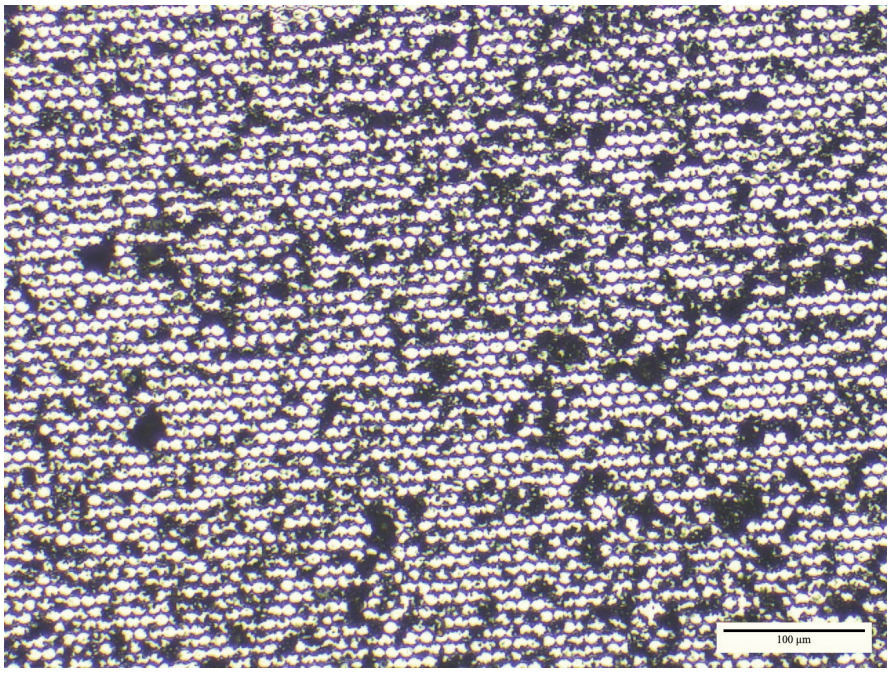

Source: Own authorship.

4.3 TRIBOLOGICAL BEHAVIOR RESULTS

Firstly, this section is dedicated to examining the tribological behavior of the varying surface conditions in terms of quantitative results identifying which surface conditions presented the highest scuffing resistance, lowest friction coefficient and highest repeatability on the scuffing resistance testing.

And in a second stage comprehending further the quantitative results on the scuffing resistance testing through the qualitative results. For this purpose, the wear mechanisms evolution was analyzed and discussed through micrographs and chemical analysis.

4.3.1 Scuffing Resistance Testing

This Section aims to discuss the quantitative results: whether the surface patterns demonstrate repeatability, weather they have a desirable scuffing resistance as for which patterns have more preferred tribological behavior.

The first stage was to determine if there was repeatability for the same patterns. Therefore, the patterns with less variability underwent a minimum of four scuffing resistance tests, while the pattern with the highest variability underwent a maximum of eight tests.

In the graphs of Figure 17 and Figure 18, the applied normal force across all tests and durability conducted are presented for each surface condition. Additionally, in these graphs is possible to draw conclusions about the level of repeatability, evidenced by the standard deviation.

Figure 22 – Average applied load.

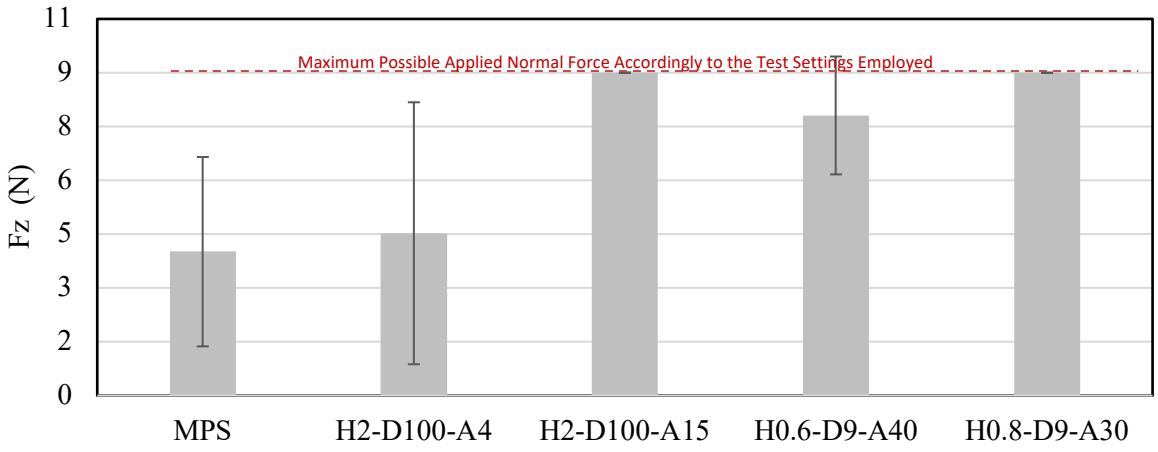

Source: Own authorship.

Figure 23 – Average Durability.

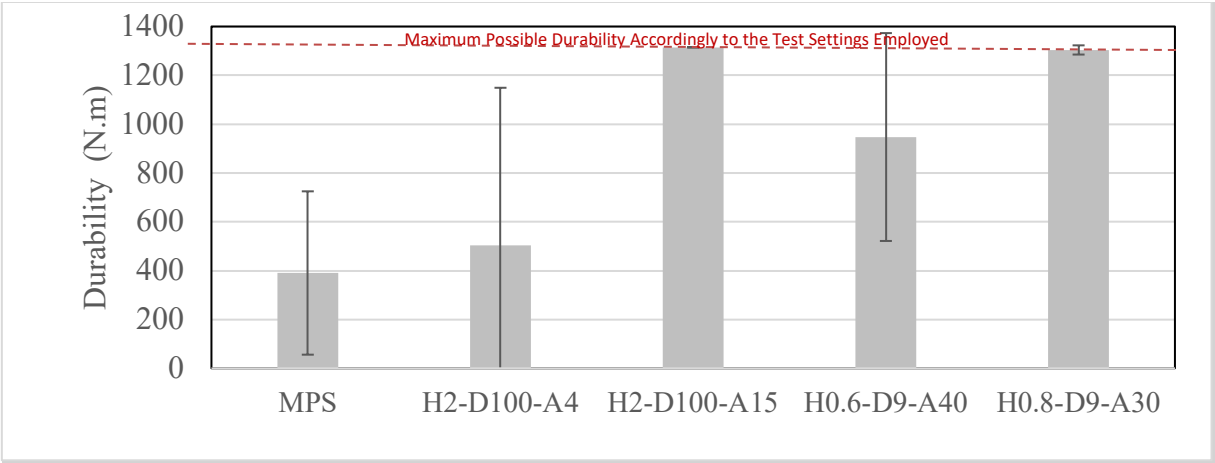

Source: Own authorship.

As shown in Figure 18, the polished surface (reference surface) and H2-D100-A4 exhibited considerable variability (low repeatability) and lower average durability compared to the other samples. It is worth noting that the significant variance in durability of H2-D100-A4, as well in friction coefficient can be attributed to certain tests where the counterpart passed directly through the dimples, leading to maximum durability and low friction coefficient, while in other tests, the counterpart passed between the dimples, resulting in lower durability and higher friction coefficient. Further exploration of this phenomenon will be discussed in the next section.

The sample H0.6-D9-A40 displayed an intermediate standard deviation when compared to all the samples as shown in Figure 18. This can be attributed to the fact that this

pattern had two tribological responses either the friction coefficient reached 0.2 (no longer in the self-lubricating regime) at 6 N (fourth load) or achieved maximum durability.

The patterns H2-D100-A15 and H0.8-D9-A30, as observed in Figure 18, demonstrated maximum durability and high repeatability as evidenced by the low standard deviation.

Therefore, the presence of dimples on the surface may result in a mechanical component at least three times more durable and reliable when compared to a common polished component, under the condition that the pattern parameters are designed correctly.

Regarding the friction coefficient, it remained consistently low throughout the lubrication regime, approximately 0.06, for the samples that demonstrated intermediate to high durability. This trend is clearly illustrated in Figure 19.

Figure 24 – Average Friction Coefficient.

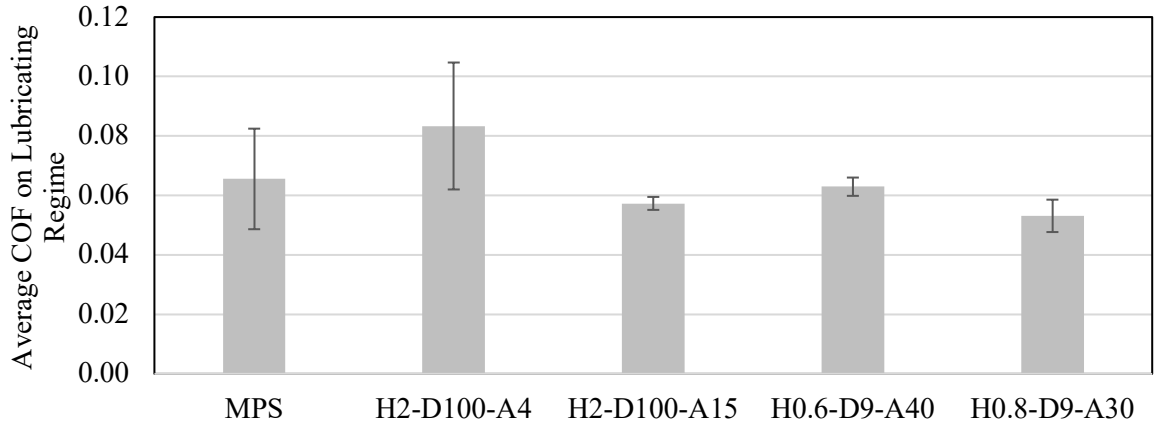

Source: Own authorship.

4.4 WEAR MECHANISMS

In the previous section was discussed the quantitative results for the scuffing resistance testing carried out. Therefore, this section aims to explore further in qualitative terms. To accomplish this, micrographs from the wear tracks and counterparts in addition to chemical analysis were performed for full-length testing, representing the condition at the end of the scuffing resistance testing, and interrupted testing at the end (8 minutes) of the second load, representing the initial condition of the scuffing resistance testing. With this approach is possible understanding the evolution of the wear mechanisms from across the five surface conditions investigated on this study.

Therefore, by compiling these micrographs that show the evolution of the wear mechanisms, the objective is to gain comprehensive understanding of the durability quantitative results discussed in the previous section. Specifically, comprehending the reason for varying durability among distinct patterns and how surface patterning may extend a component's lifespan when compared to conventional polished component.

4.4.1 Mirror-Polished Surface Evolution of Wear Mechanisms

The mirror polished surface (reference surface) condition had varying, and low durability as shown in Figure 18 from the previous section. The wear evolution for this surface is shown in Figure 20. In image "a" is presented the wear track after an interrupted testing, the interrupted testing represents the initial state of the wear mechanism during scuffing resistance testing. Notably, the formation of a tribofilm is evident by the smooth aspect in contrast to the surrounding substrate. Additionally, there is an evident accumulation of 2D turbostratic graphite (CDC) particles at the edge of the track and an absence of CDC particles on the track itself. This observation suggests that as the scuffing resistance testing progresses, CDC particles are swept from the wear track and accumulate at the edge of the track. This accumulation of solid lubricant appears to serve as a source of lubrication for the tribofilm, contributing to maintaining a low friction coefficient and consequently lubricity while there is the existence of these solid lubricant reservoirs at the edge of the wear track.

Figure 25 – Optical Microscope Micrographs of Mirror-Polished Wear Tracks at 100x Magnification. (a) Wear track obtained after an interrupted scuffing resistance testing at 8 minutes into the second load. (b) Wear track obtained after the full-length scuffing resistance testing.

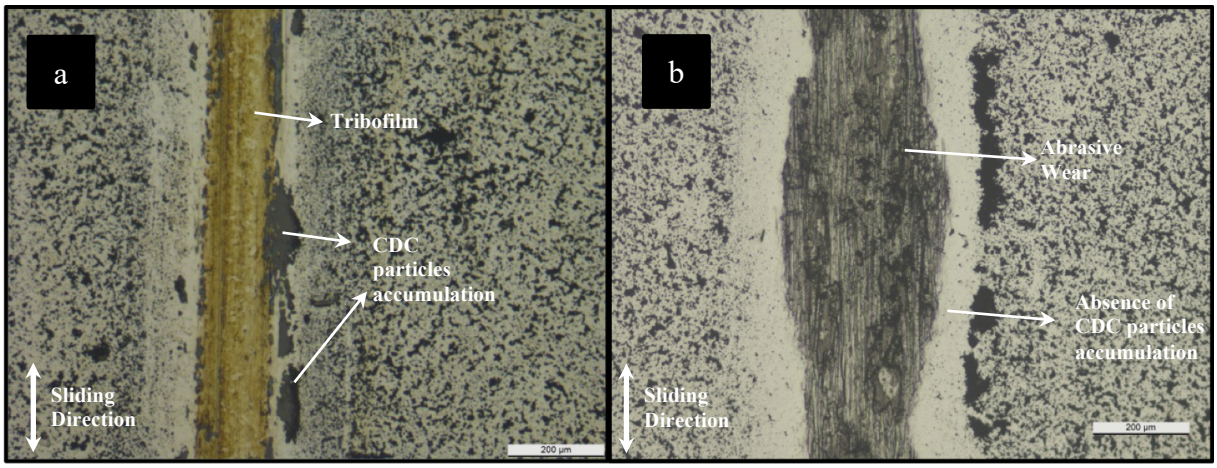

Source: Own authorship.

In the previous Figure 20 “b”, a micrograph of the wear track was taken after a full-length testing, when the polished surface transitioned out of the self-lubrication regime (indicated by the COF overpassing 0.2), reveals severe abrasive wear characterized by scratches and debris on the wear tracks confirmed by the composition analysis in Figure 21, which shows that the particles are clearly debris since they present oxygen content. Notably, the CDC particles accumulation is observed further from the edge of the track compared to the interrupted testing in Figure 20 “a”, indicating that all remained solid lubricant supply at the edge of the track ran out. Consequently, there was no longer a source of solid lubricant supply to sustain the tribofilm and, subsequently, lubricity.

Figure 26 – Composition Analysis of the Wear Track Using EDX for the Mirror-Polished Sample. (a) SEM micrography of the Debris. (b) Compositional spectrum for the stainless steel substrate. (c) Compositional spectrum for the debris. (d) Compositional spectrum for the debris.

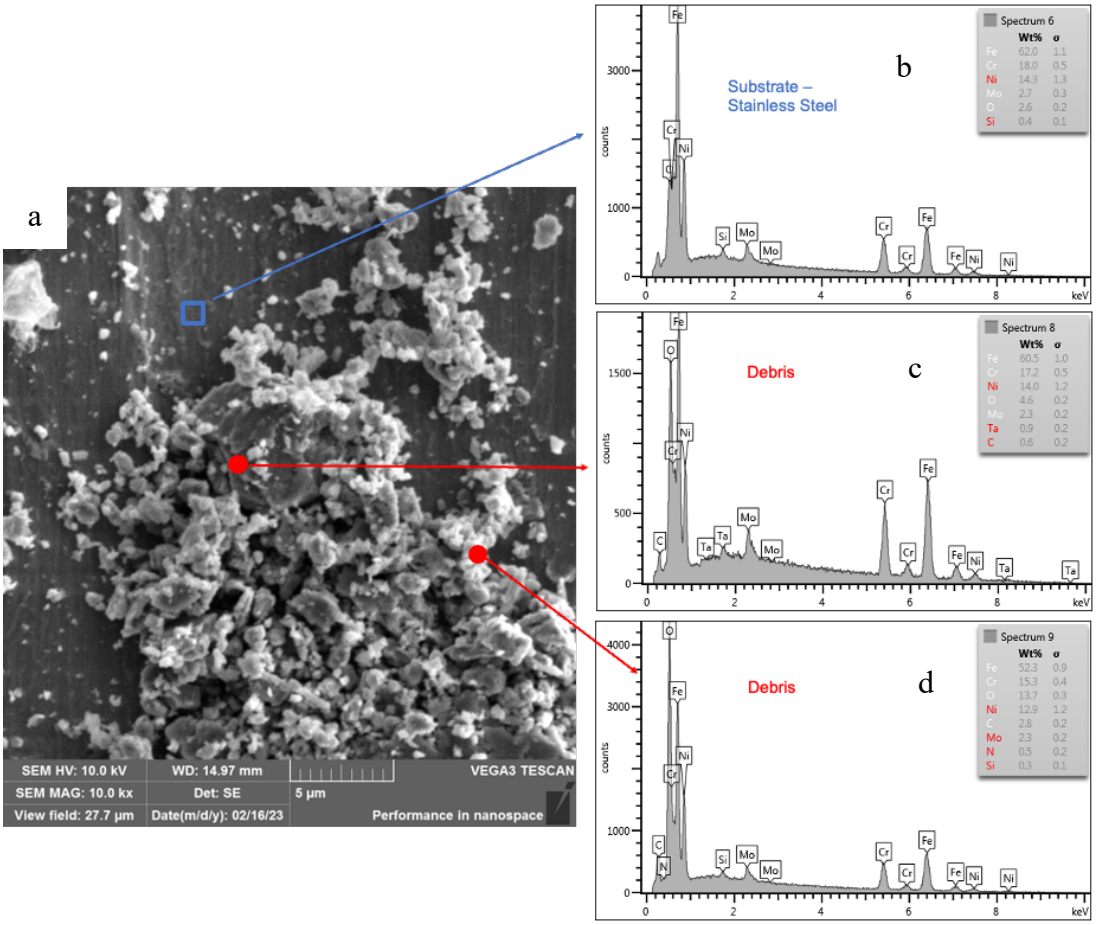

Source: Own authorship.

This surface condition exhibited a lack of repeatability in terms of durability, as discussed on the previous section. This variability in performance can be attributed to the unpredictable distribution of CDC particles agglomeration at the edge of the track that serve as a supply. Since the CDC particles reservoirs at the edge of the track could not be precisely regulated or controlled, it resulted in the lack of consistent performance across the multiple test runs.

Regarding the wear marks on the counterparts, the wear mark resulting from the interrupted testing as seen in Figure 22 “a” is relatively small and a tribofilm formed just as on

the wear track, however for the full-length testing shown in Figure 22 “b”, the wear mark is larger and abrasive wear is evident.

Figure 27 - Optical Microscope Micrographs of Mirror-Polished Counterparts at 100x Magnification. (a) Wear mark obtained after an interrupted scuffing resistance testing at 8 minutes into the second load. (b) Wear mark obtained after the full-length scuffing resistance testing.

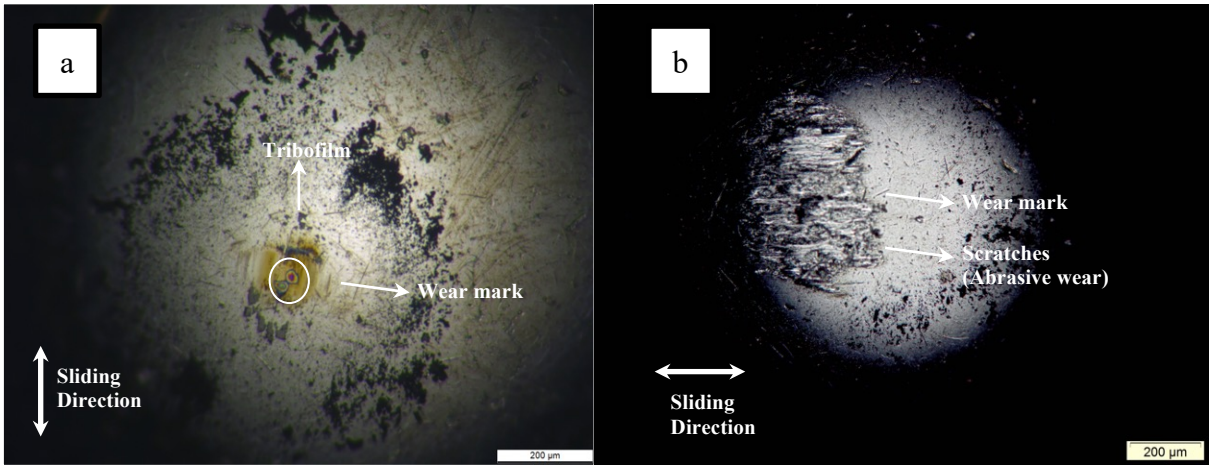

Source: Own authorship.

4.4.2 Evolution of Wear Mechanism for H2-D100-A4 pattern

H2-D100-A4 pattern exhibited the most significant variability in terms of durability, primarily attributed to its low dimples’ density in this pattern (the dimples were more spaced between each other). As a consequence, the placement of the counterpart varied across the tests conducted, either the counterpart crossed the center of the dimples, or in between them or partially over the dimples as observed in Figure 23. This led to various durability results.

The scuffing resistance tests in which the counterpart crossed the center of the dimples demonstrated great performance, as evident in the micrograph in Figure 23 “c” and its scuffing resistance testing graph in Figure 23 “f”, as the dimples effectively acted as solid lubricant reservoirs. Otherwise, if the counterpart did not cross the center of the dimples, it resulted in poor performance, as observed in the micrographies from Figure 23 “a”, “b”, and its corresponding scuffing resistance testing graphs in Figure 23 “d”, and “e”.

Figure 28 – Optical Microscope Micrographs at 100x Magnification of the Wear Tracks Resulting from Full-length Scuffing Resistance Tests on the H2-D100-A4 pattern and its corresponding Scuffing Resistance Testing Graphs. (a) Wear track between dimples. (b) Wear track between dimples. (c) Wear track passing across the dimples. (d) Scuffing resistance testing graph from the corresponding wear track in image “a”. (e) Scuffing resistance testing graph from the corresponding wear track in image “b”. (f) Scuffing resistance testing graph from the corresponding wear track in image “c”.

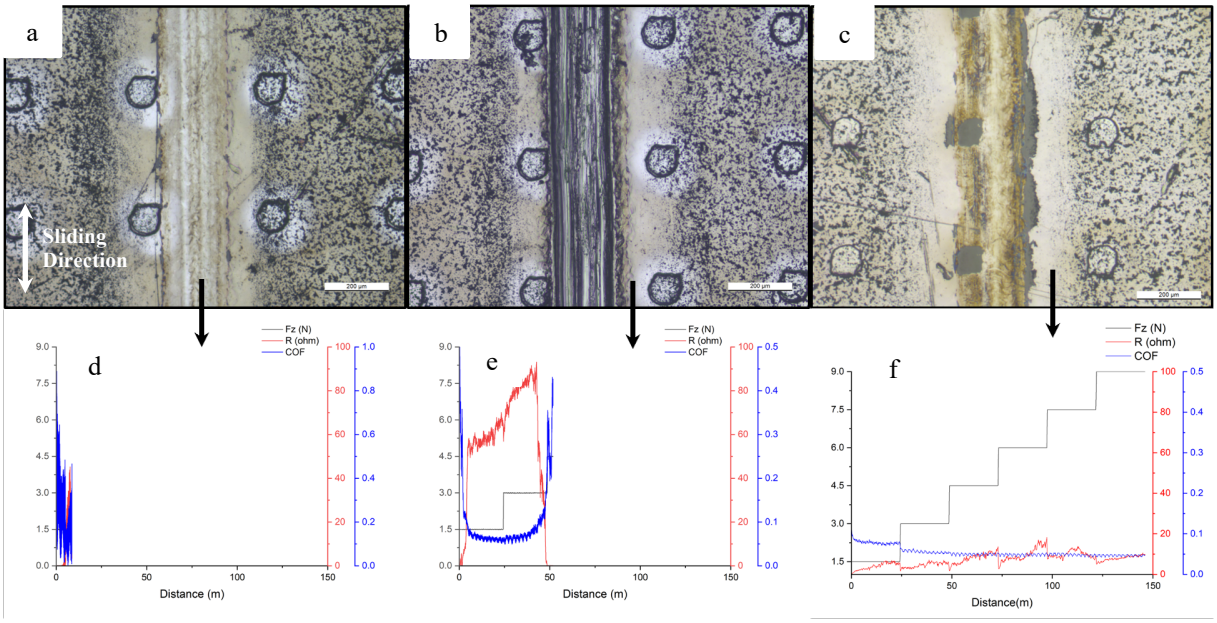

Source: Own authorship.

These observations clearly show the critical lubrication role of the dimples, acting as lubricant reservoirs that gradually supply lubricant, ensuring consistent lubrication. Instances where the counterpart did not cross the dimples lacked this lubrication mechanism, leading to diminished performance in these samples.

The chosen testing configuration, employing a sphere against a plane and resulting in a "line" wear track, imposes a severe wear condition characterized by high contact pressure.

Wear conditions are typically less severe, and the resulting wear track is usually wider. In such scenarios, the sample could experience enhanced lubrication benefits owing to the wider track area. This wider area facilitates a more consistent interaction between the dimples on the sample's surface and the counterpart. Consequently, in these conditions, the dimples have the potential to establish a continuous and consistent supply of solid lubricant, functioning as reliable reservoirs.

Furthermore, due to the variability in the positioning of the counterpart, resulting from the low pattern density, it was not possible to draw any conclusion regarding the underlying wear mechanisms evolution.

4.4.3 Evolution of Wear Mechanism for H2-D100-A15 pattern

The H2-D100-A15 pattern, characterized by identical pattern parameters to the previously discussed pattern except for a higher packing density (15%), consistently demonstrated maximum durability, as demonstrated in Figure 18 from the previous section. The wear evolution for this surface is presented in Figure 24. Image “a” demonstrates the wear track after an interrupted testing, revealing the dimples have experienced minimal wear and CDC particles accumulation is observed in some dimples, although not in all dimples along the wear track. Additionally, there are areas of CDC particles accumulation at the edge of the track.

Figure 24 “b” and Figure 25 show the wear track’s appearance following a full-length scuffing resistance testing. It is apparent that the dimples have undergone wear, but they are still existent and acting as lubricant reservoirs. However, there is a noticeable reduction in the accumulated CDC particles stored on the dimples compared to the interrupted testing. This reduction suggests that the CDC particles have been partially utilized during the testing, which explain lubricity and consequently sustained durability observed in this pattern. Additionally, there are more areas of CDC particles accumulation at the edge of the track compared to the interrupted testing.

Figure 29 – Optical Microscope Micrographs of H2-D100-A15 Pattern Wear Tracks at 100x Magnification. (a) Wear track obtained after an interrupted scuffing resistance testing at 8 minutes into the second load. (b) Wear track obtained after the full-length scuffing resistance testing.

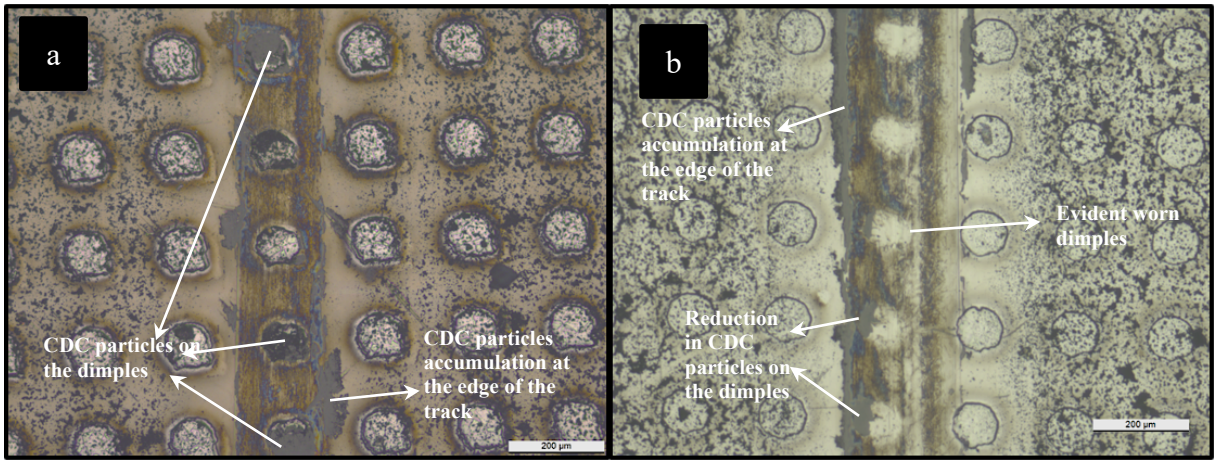

Source: Own authorship.

Figure 30 – Scanning Electron Microscope Micrographs at 500x Magnification Resulting from Full-length Scuffing Resistance Test on the H2-D100-A15 Pattern.

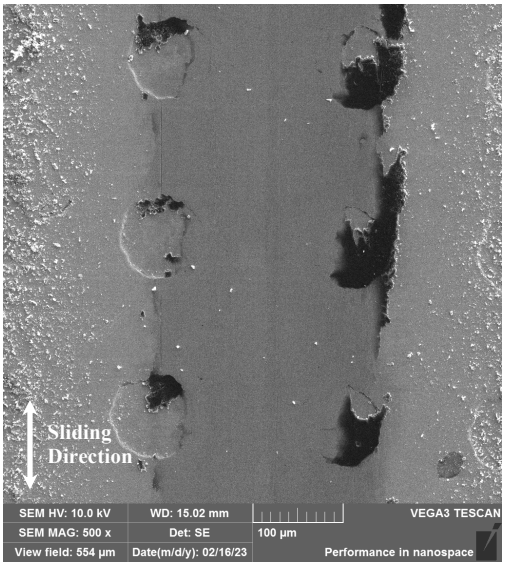

Source: Own authorship.

As for the counterpart, the difference between the interrupted testing and the full-length testing is that a tribofilm on the counterpart has not formed for the interrupted testing as observed in Figure 26 “a”. While, for full-length scuffing resistance testing a tribofilm has clearly formed, as observed in Figure 26 “b”.

Figure 31 - Optical Microscope Micrographs of Mirror-Polished Counterparts at 100x Magnification. (a) Wear mark obtained following an interrupted scuffing resistance testing at 8 minutes into the second load. (b) Wear mark obtained following the full-length scuffing resistance testing.

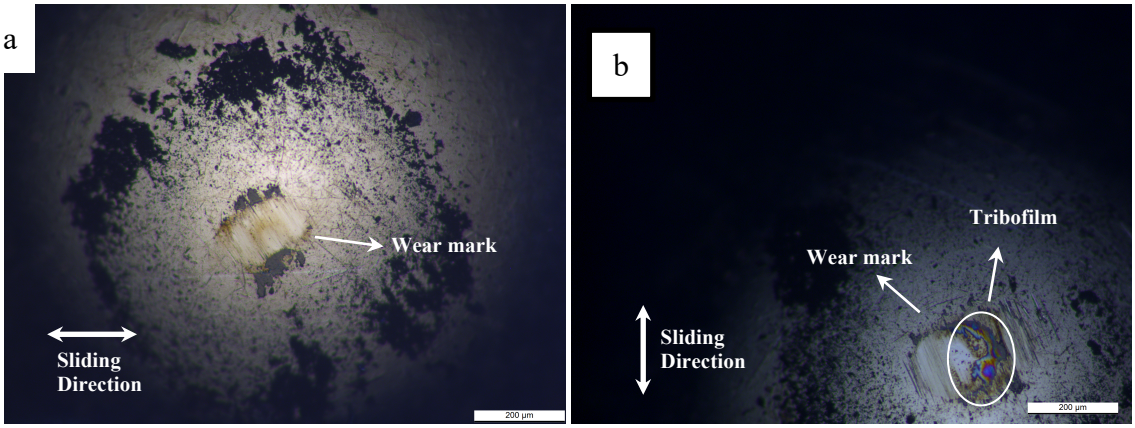

Source: Own authorship.

4.4.4 Evolution of Wear Mechanism for H0.6-D9-A40 and H0.8-D9-A30 patterns

The H0.6-D9-A40 and H0.8-D9-A30 patterns will be addressed simultaneously due to their similarities; both feature smaller and more closely packed dimples compared to the previously discussed patterns. Remarkably, these patterns consistently achieved maximum durability, except for H0.6-D9-A40, which occasionally did not achieve maximum durability, as demonstrated in Figure 18 from the previous section.

Figure 27 “a” and “b” show the wear track of the pattern H0.6-D9-A40 after an interrupted testing, revealing that a great number of dimples are filled with CDC particles. As a result, these patterns have high durability because the dimples effectively act as reservoirs, supplying nanolubricant for the formation and maintenance of a tribofilm. The presence of the nanolubricant on the dimples and the formation tribofilm has been confirmed by the composition analysis in Figure 29.

Figure 32 – Optical Microscope Micrographs of H0.6-D9-A40 Wear Tracks at 200x (a) and 500x (b) Magnification.

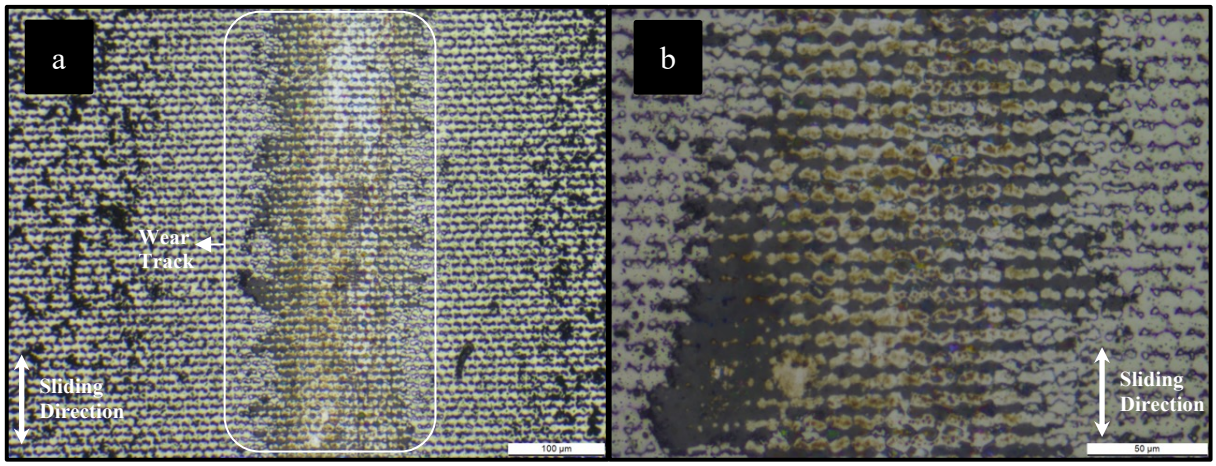

Source: Own authorship.

Figure 28 and Figure 29 show the wear tracks and composition analysis following a full-length scuffing resistance testing conducted in H0.6-D9-A40 and H0.8-D9-A30 patterns. Notably, due to the patterns' similarity, the wear tracks reassemble each other. It becomes apparent that, at this stage of testing (end of the testing), the dimples are more worn, and CDC particles agglomeration at the edge of the track is more evident. This occurs because as the dimples gradually wear down, the surface begins to resemble the polished sample, resulting in a shift towards similar wear mechanisms. Therefore, if the testing could extend beyond 9 N, it would likely continue until the dimples were entirely worn, and all the CDC supply at the edge of the track was consumed, as discussed for the wear mechanism evolution for the polished surface in Section 4.4.1.

Figure 33 – Optical Microscope Micrographs of H0.6-D9-A40 (a) and H0.8-D9-A30 (b) Wear Tracks at 200x Magnification.

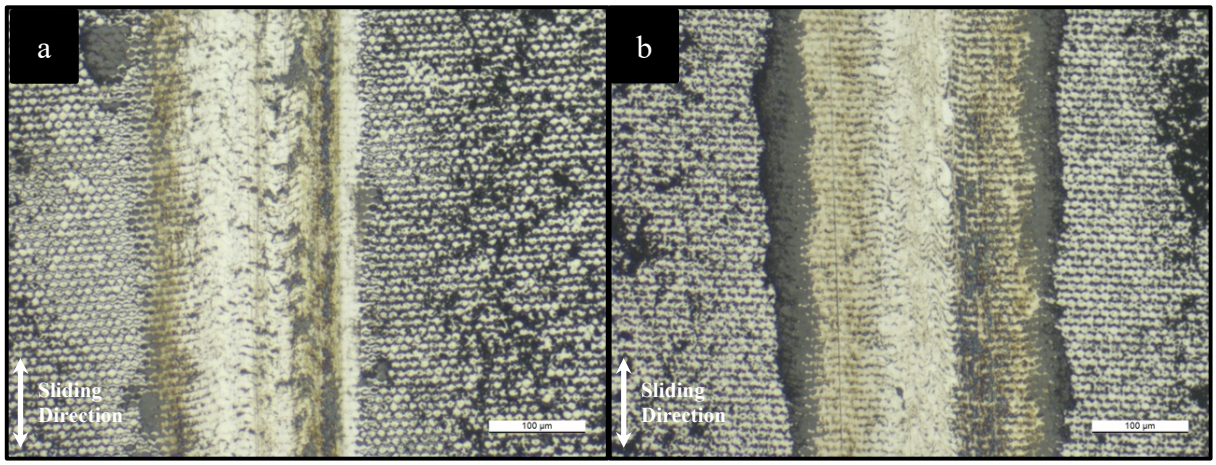

Source: Own authorship.

Figure 34 – Composition Analysis of the Wear Track Using EDX for the H0.6-D9-A40 Pattern. (a) SEM micrography of the wear track. (b) Compositional spectrum for the stainless steel substrate. (c) Compositional spectrum for the solid nanolubricant on the dimples. (d) Compositional spectrum for the tribofilm. (e) Compositional spectrum for the tribofilm.

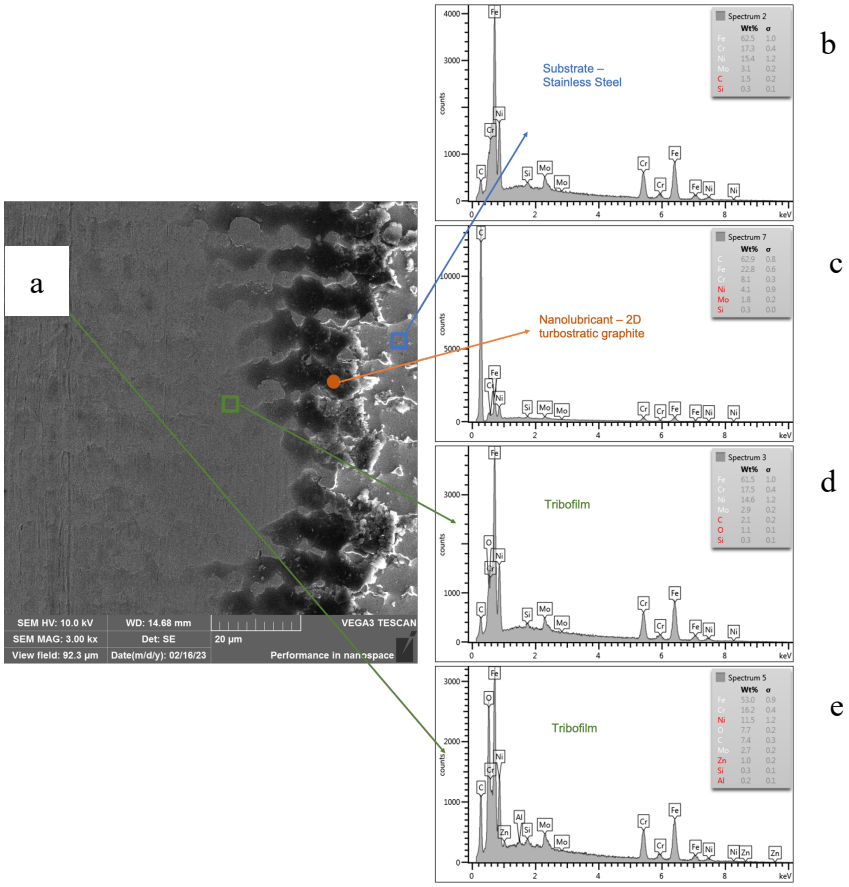

Source: Own authorship.

H0.6-D9-A30 pattern occasionally failed to reach maximum durability, this occurrence may be attributed to the slightly shorter dimples for this pattern.

As for the counterpart, at the beginning of the scuffing resistance testing, a small clear wear mark is observed with no presence of a tribofilm, as observed in Figure 30 “a”. While, at end of the scuffing resistance testing a tribofilm has clearly formed, and the wear mark remained close to the initial size, as observed in Figure 30 “b”.

Figure 35 - Optical Microscope Micrographs of Mirror-Polished Counterparts at 100x Magnification. (a) Wear mark obtained following an interrupted scuffing resistance testing at 8 minutes into the second load. (b) Wear mark obtained following the full-length scuffing resistance testing.

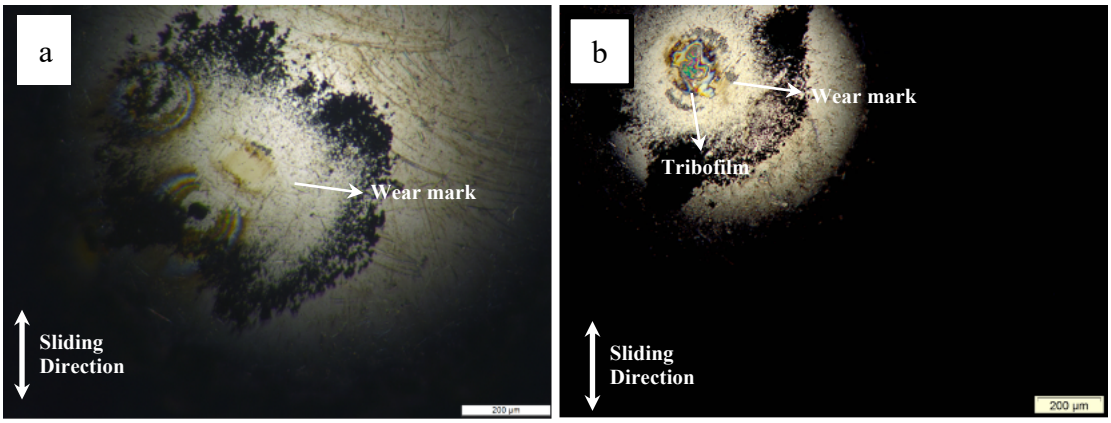

Source: Own authorship.

4.5 RAMAN ANALYSIS OF TRIBOFILMS

In order to further understand the evolution of wear mechanisms and structural changes in the solid lubricant following the scuffing resistance testing on different patterns, Raman spectroscopy measurements were performed on the 2D turbostratic graphite powder used and on the wear track after the scuffing resistance testing.

The spectra for the different surface conditions and the solid nanolubricant powder utilized in this analysis are presented in Figure 31. These spectra allow the identification of the first-order bands and second-order bands. A comparison between the 2D turbostratic graphite particles spectrum and the Raman spectra of the patterned surfaces after the scuffing resistance testing reveals that the 2D band decreases its intensity and the D+G band increases its intensity.

This observation suggests that the friction and the pressure of the scuffing resistance testing possibly caused higher shearing of the carbon layers of the 2D structure, as the 2D band intensity decreased, since the band is associated with the stacking layers of the carbon structure. In addition, D+G band, linked to distortions and defects, increases, indicating more defects on the carbon structure (NEVES et al., 2024).

Figure 36 – Raman Spectra of the solid nanolubricant powder, H2-D100-A4 pattern, and H2-D100-A15.

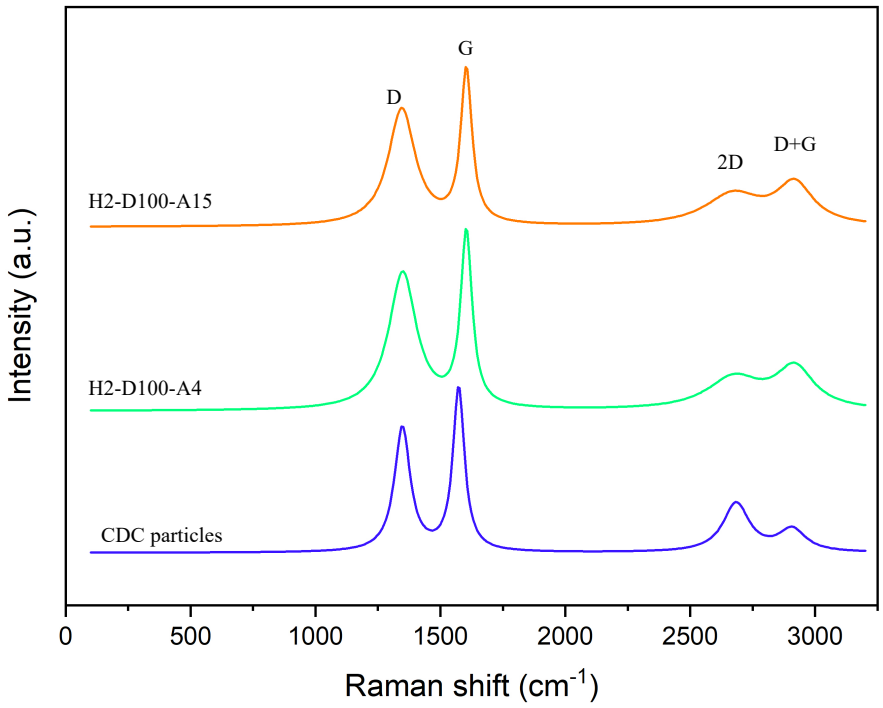

Source: Own authorship.

The scuffing resistance testing increased the disorder and defects of the 2D turbostratic graphite, regardless of the patterns. Table 6 clearly shows this as the FWHM values for D, 2D, and D+G bands increased in comparison to the CDC powder, and the ratio I_D/I_G is also slightly higher than the original material, underlining the increase in presence of defects.

Table 6 - Data of the Raman spectra bands of the carbon present on the tribofilms.

	D		G		2D		D+G		I_D/I_G
	Pos	FWHM	Pos	FWHM	Pos	FWHM	Pos	FWHM	
CDC particles	1347	68.2	1572	50.8	2683	123.5	2909	127.1	0.73
H2-D100-A4	1347	122.7	1603	55.0	2678	258.3	2920	179.6	0.78
H2-D100-A15	1350	126.1	1603	53.2	2669	254.8	2916	195.1	0.75

Source: Own authorship.

The representative spectra, illustrating the deconvolution of the overlapping bands corresponding the surface conditions under consideration, are displayed in Figure 32. The D3 band becomes distinctly evident following the deconvolution process, and it is associated with the amorphous component of the material.

Figure 37– Representative Raman Spectra afterwards the Deconvolution. (a) CDC particles representative spectrum. (b) H2-D100-A4 and H2-D100-A4 patterns representative spectrum.

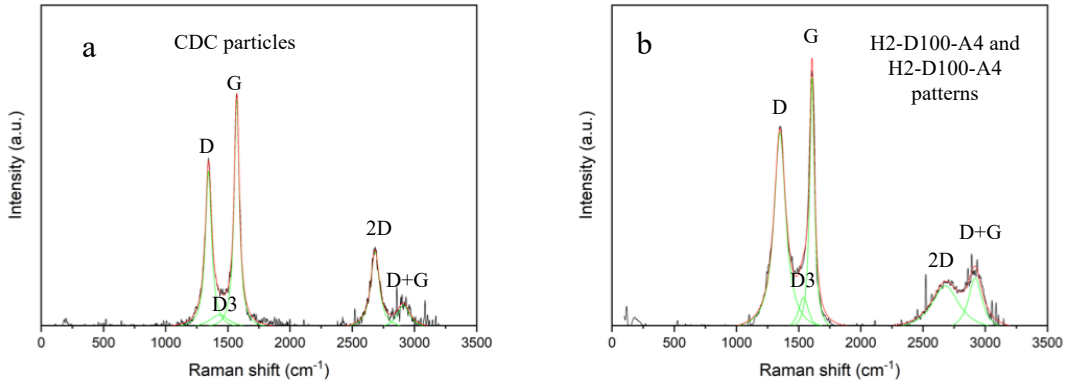

Source: Own authorship.

5 CONCLUSION

In summary, this study successfully implemented both surface patterning technology and nanolubricant deposition, allowing for a comprehensive investigation into their combined impact on tribological behavior. The key findings and conclusions from the tribological analysis of the different surface conditions are as follows:

1- Reference Surface (Mirror-Polished Finish): The reference surface exhibited poor tribological performance with low durability and repeatability. This was attributed to the accumulation of CDC particles at the edge of the track, these CDC particles agglomeration could not be controlled and predicted, consequently lead to inconsistent outcomes.

2- H2-D100-A4 Pattern: This pattern also presented poor tribological behavior results due to its low dimples area density, meaning that the dimples were more spaced between each other. Consequently, the counterpart did not consistently pass through the center of the dimples, resulting in varying wear patterns.

3- H2-D100-A15 Pattern: In contrast, the H2-D100-A15 pattern, which featured the same pattern parameters as H2-D100-A4 pattern but with a higher area density of 15%, exhibited remarkable durability and repeatability. For this condition, the counterpart consistently traversed the dimples, enabling them to act as CDC particle reservoirs that gradually supplied lubricant throughout the testing. Even at the test's conclusion, the dimples remained, although little worn and with reduced CDC particle quantity.

4- Small Dimples Patterns (H0.6-D9-A40 and H0.8-D9-A30): These patterns showcased maximum durability, except for H0.6-D9-A40 which in some instances, achieved intermediate durability. Initially, various dimples were filled with CDC particles. However, as the testing continued, the dimples gradually wore down, and the track began to resemble the wear track seen on a polished surface. This closer resemblance to the polished surface resulted in an increased agglomeration of CDC particles at the edge of the track and a decrease in the number of dimples accumulating CDC particles along the track.

In conclusion, this study demonstrates the synergistic potential of combining surface patterning and solid nanolubricant deposition to effectively reduce wear and friction. Well-designed patterns on the surface can enhance durability and repeatability significantly, it is

worth noting that in our study, the patterned surfaces (except for H2-D100-A4 pattern) exhibited exceptional durability, with the patterns outperforming the common mirror-polished sample's durability by a factor of at least three. Furthermore, the dimples act as reservoirs, gradually supplying lubricant to sustain the tribofilm as they wear, ultimately contributing to improved tribological performance and generally enhancing repeatability compared to polished surface as they offer a level of surface control that ensures a more consistent and predictable performance. Additionally, the wear mechanisms observed suggest that as the patterns wear down, they transition toward resembling the polished surface, with CDC particles accumulating more at the edge of the track.

Therefore, incorporating surface patterning could be beneficial for tribological systems already leveraging solid lubricant particles. Both H0.8-D9-A30 and H2-D100-A15 patterns demonstrated remarkable durability and low variability. However, at the end of the durability tests performed, H2-D100-A15 pattern was still well preserved, although showing signs of wear, while H0.8-D9-A30 pattern was almost completely worn. Having said that, for more severe wear conditions, H2-D100-A15 pattern could be more appropriate. Additionally, there is potential for further optimization by introducing dimples with a slightly increased depth, which could enhance the performance of this pattern even further.

6 SUGGESTIONS FOR FUTURE RESEARCH

The developed methodologies and the promising results observed present opportunities for future research, such as:

- Conducting friction tests under other conditions, such as modifying the geometry of the counterpart and altering the testing motion. This exploration aims to comprehensively understand the influence of these parameters on the tribological behavior of the patterns.
- Replicating the durability tests using an equipment capable of achieving higher durability, therefore enabling a further examination of wear mechanism evolution for patterns that demonstrated maximum durability.
- Study the influence of the nanoparticle's coverage in tribological behavior and, concluding if there is an optimal coverage.
- Exploring the utilization of alternative materials for both the sample and lubricant particles to assess if similar results can be achieved under different material combinations.

REFERENCES

AGUILAR-MORALES, A. I. et al. Influence of processing parameters on surface texture homogeneity using Direct Laser Interference Patterning. **Optics & Laser Technology**, v. 107, p. 216–227, nov. 2018.

BASHER, M. K. et al. Study and analysis the Cu nanoparticle assisted texturization forming low reflective silicon surface for solar cell application. **AIP Advances**, v. 9, n. 7, p. 075118, jul. 2019.

BISWAS, S. et al. Effect of ultrasonic vibration-assisted laser surface melting and texturing of Ti-6Al-4V ELI alloy on surface properties. **Journal of Materials Science & Technology**, v. 35, n. 2, p. 295–302, fev. 2019.

Britannica. Solid lubricants. 2020. Disponível em: https://www.britannica.com/technology/lubrication/Solid-lubricants. Accessed in: 24/05/2023.

BRUZZONE, A. A. G. et al. Advances in engineered surfaces for functional performance. **CIRP Annals**, v. 57, n. 2, p. 750–769, 2008.

CHEN, L. et al. Surface Characterization and Tribological Performance of Anodizing Micro-Textured Aluminum-Silicon Alloys. **Materials**, v. 12, n. 11, p. 1862, 9 jun. 2019.

CHEN, L.; LIU, Z.; SHEN, Q. Enhancing tribological performance by anodizing micro-textured surfaces with nano-MoS2 coatings prepared on aluminum-silicon alloys. **Tribology International**, v. 122, p. 84–95, jun. 2018.

COBLAS, D. G. et al. Manufacturing textured surfaces: State of art and recent developments. **Proceedings of the Institution of Mechanical Engineers, Part J: Journal of Engineering Tribology**, v. 229, n. 1, p. 3–29, jan. 2015.

CONRADS, H.; SCHMIDT, M. Plasma generation and plasma sources. **Plasma Sources Science and Technology**, v. 9, n. 4, p. 441–454, 1 nov. 2000.

ERDEMIR, A. **Solid Lubricants and Self-Lubricating Films**. 2001.

ERDEMIR, A. Vol. 22 - **Solid lubricants and Self-lubricating films.** In: BHUSHAN, B. (Ed.). Modern Tribology Handbook. 1. ed. CRC Press, 2001. p. 787–818.

FAN, H. et al. Design of “double layer” texture to obtain superhydrophobic and high wear-resistant PTFE coatings on the surface of Al2O3/Ni layered ceramics. **Tribology International**, v. 136, p. 455–461, ago. 2019.

FARIA, D. et al. Novel laser textured surface designs for improved zirconia implants performance. **Materials Science and Engineering: C**, v. 108, p. 110390, mar. 2020.

GENG, H. (ED.). **Semiconductor manufacturing handbook**. New York: McGraw-Hill, 2005.

GIACOMELLI, Renan Oss. **Metodologia para investigação do desempenho tribológico de nanopartículas de lubrificantes sólidos na macroescala aplicada a grafeno e carbono derivado de carbetos.** 2020. Tese (Doutorado). Programa de Pós-Graduação em Ciência e Engenharia de Materiais, Universidade Federal de Santa Catarina.

HOLMBERG, K.; ERDEMIR, A. Influence of tribology on global energy consumption, costs and emissions. **Friction**, v. 5, n. 3, p. 263–284, set. 2017.

HUA, X. et al. Tribological Properties of Laser Microtextured Surface Bonded With Composite Solid Lubricant at High Temperature. **Journal of Tribology**, v. 138, n. 3, p. 031302, 1 jul. 2016.

HUANG, Q. et al. Recent progress on surface texturing and solid lubricants in tribology: Designs, properties, and mechanisms. **Materials Today Communications**, v. 35, p. 105854, jun. 2023.

IBATAN, T.; UDDIN, M. S.; CHOWDHURY, M. A. K. Recent development on surface texturing in enhancing tribological performance of bearing sliders. **Surface and Coatings Technology**, v. 272, p. 102–120, jun. 2015.

JAIN, A.; BAJPAI, V. Mechanical micro-texturing and characterization on Ti6Al4V for the improvement of surface properties. **Surface and Coatings Technology**, v. 380, p. 125087, dez. 2019.

JEYAPRAKASH, N.; YANG, C.-H. Friction, Lubrication, and Wear. Em: PATNAIK, A.; SINGH, T.; KUKSHAL, V. (Eds.). **Tribology in Materials and Manufacturing - Wear, Friction and Lubrication**. [s.l.] IntechOpen, 2021.

JOST, H. P. Tribology Micro & Macro Economics: A Road to Economic Savings. **Tribology and Lubrication Technology**, v. 61, n. 10, p. 18, 2005.

KUMAR, C. S. S. R. (ED.). **Raman spectroscopy for nanomaterials characterization; with 11 tables**. Berlin Heidelberg: Springer, 2012.

LE DAIN, G. et al. Etching of iron and iron–chromium alloys using ICP-RIE chlorine plasma. **Plasma Sources Science and Technology**, v. 30, n. 9, p. 095022, 1 set. 2021.

MANOS, D. M.; FLAMM, D. L. **Plasma etching: an introduction**. Boston: Academic Press, 1989.

MARSH, H.; RODRÍGUEZ-REINOSO, F. Production and Reference Material. Em: **Activated Carbon**. [s.l.] Elsevier, 2006. p. 454–508.

MIYOSHI, K. K. **Solid Lubrication Fundamentals and Applications**. 1st. ed. Cleveland: CRC Press, 2001. v. 20014823

NEVES, G. O. **Síntese de Partículas de Carbono Nanoestruturado Através da Reação entre Carbetos Precursores Distintos.** 2020. Tese (Doutorado). Programa de Pós- Graduação

em Ciência e Engenharia de Materiais, Universidade Federal De Santa Catarina**,** Florianópolis, 2020.

NEVES, G. O. et al. Tribologically induced nanostructural evolution of carbon materials: A new perspective. **Friction**, v. 12, n. 1, p. 144–163, jan. 2024.

OBILOR, A. F. et al. Micro-texturing of polymer surfaces using lasers: a review. **The International Journal of Advanced Manufacturing Technology**, v. 120, n. 1–2, p. 103–135, maio 2022.

ORLAND, A. S.; BLUMENTHAL, R. Metal etching with organic based plasmas. II. CO⁄NH[sub 3] plasmas. **Journal of Vacuum Science & Technology B: Microelectronics and Nanometer Structures**, v. 23, n. 4, p. 1597, 2005.

PETTERSSON, U.; JACOBSON, S. Textured surfaces for improved lubrication at high pressure and low sliding speed of roller/piston in hydraulic motors. **Tribology International**, v. 40, n. 2, p. 355–359, fev. 2007.

PRESSER, V.; HEON, M.; GOGOTSI, Y. Carbide-derived carbons - from porous networks to nanotubes and graphene. **Advanced Functional Materials**, v. 21, n. 5, p. 810–833, 2011.

QIU, M.; LI, Y.; CHEN, L.; YAN,J. Bearing Tribology: Principles and Applications. 1 ed., 2017.

RAPOPORT, L. et al. Friction and wear of MoS2 films on laser textured steel surfaces. **Surface and Coatings Technology**, v. 202, n. 14, p. 3332–3340, abr. 2008.

RIPOLL, M. R. et al. Friction and Lifetime of Laser Surface–Textured and MoS2-Coated Ti6Al4V Under Dry Reciprocating Sliding. **Tribology Letters**, v. 51, n. 2, p. 261–271, ago. 2013.

ROSENKRANZ, A. et al. Synergetic effects of surface texturing and solid lubricants to tailor friction and wear – A review. **Tribology International**, v. 155, p. 106792, mar. 2021.

SEDLAČEK, M.; GREGORČIČ, P.; PODGORNIK, B. Use of the Roughness Parameters S_{sk} and S_{ku} to Control Friction—A Method for Designing Surface Texturing. **Tribology Transactions**, v. 60, n. 2, p. 260–266, 4 mar. 2017.

SEGU, D. Z. et al. Application of Taguchi techniques to study friction and wear properties of MoS2 coatings deposited on laser textured surface. **Surface and Coatings Technology**, v. 232, p. 504–514, out. 2013.

SREEJITH, K. P. et al. Etching methods for texturing industrial multi-crystalline silicon wafers: A comprehensive review. **Solar Energy Materials and Solar Cells**, v. 238, p. 111531, maio 2022.

STACHOWIAK, G. BATCHELOR, A. W. **Engineering Tribology.** 3rd Edition. Elsevier Buttenworth- Heinemann, 2005.

SUI, J.; LU, J. Formulated self-lubricating carbon coatings on carbide ceramics. **Wear**, v. 271, n. 9–10, p. 1974–1979, jul. 2011.

TALA-IGHIL, N.; FILLON, M.; MASPEYROT, P. Effect of textured area on the performances of a hydrodynamic journal bearing. **Tribology International**, v. 44, n. 3, p. 211–219, mar. 2011.

URBONAITE, S.; HÄLLDAHL, L.; SVENSSON, G. Raman spectroscopy studies of carbide derived carbons. **Carbon**, v. 46, n. 14, p. 1942–1947, nov. 2008.

VENCL, A. et al. SURFACE TEXTURING FOR TRIBOLOGICAL APPLICATIONS: A REVIEW. **Proceedings on Engineering Sciences**, v. 1, n. 1, p. 227–239, maio 2019.

VISHNOI, M.; KUMAR, P.; MURTAZA, Q. Surface texturing techniques to enhance tribological performance: A review. **Surfaces and Interfaces**, v. 27, p. 101463, dez. 2021.

VOEVODIN, A. A.; ZABINSKI, J. S. Laser surface texturing for adaptive solid lubrication. **Wear**, v. 261, n. 11–12, p. 1285–1292, dez. 2006.

WANG, S.; SHAO, G. Silicon Carbide-Derived Carbon Prepared by Fused Salt Electrolysis and Electrochemical Performance. **Journal of Nanomaterials**, v. 2016, 2016.

ZHANG, K. et al. Effect of ion beam etching on the tribological performance of laser textured Co-Cr-Mo alloy. **Optics & Laser Technology**, v. 160, p. 109097, maio 2023.
ZUM GAHR, K.-H. **Microstructure and wear of materials**. Amsterdam: Elsevier, 2010.